PROBABILISTIC DETERMINATION OF BRAIN TUMOR LOCATIONS

by

Yasin Çotur

BS, in Electrical & Electronics Engineering, Boğaziçi University, 2013

Submitted to the Institute of Biomedical Engineering
in partial fulfillment of the requirements
for the degree of
Master of Science
in
Biomedical Engineering

Boğaziçi University
2015

PROBABILISTIC DETERMINATION OF BRAIN TUMOR LOCATIONS

APPROVED BY:

Prof. Dr. Mehmed ÖZKAN .....
(Thesis Advisor)

Adj. Prof. Dr. Aziz M. ULUĞ .....
(Thesis Co-advisor)

Prof. Dr. Albert GÜVENİŞ .....

Assist. Prof. Dr. Esin ÖZTÜRK IŞIK .....

Assist. Prof. Dr. Ali Emre PUSANE .....

DATE OF APPROVAL: 28 July 2015

ACKNOWLEDGMENTS

First of all, I would like to thank my advisor, Prof. Mehmed Özkan, for his encouragement, generous help and guidance throughout my project and also throughout my education.

I also would like to thank Adj. Prof. Aziz M. Uluğ, for his guidance and support throughout my thesis and crucial role he played in planning my thesis.

In addition, I would like to thank my friend, Ali Demir for his support and encouragement. Also, I want to thank to MD. Hale Turnaoğlu, MD. Ahmet Muhteşem Ağıldere, and MD. Özlem Alkan from Başkent University Medical School, MD. Mutlu Cihangiroğlu and Andaç Hamamcı from Yeditepe University for their technical support.

Finally, I would like to thank my wife, Merve Çirişoğlu Çotur who has always been there for her endless support, love and encouragement.

ABSTRACT

PROBABILISTIC DETERMINATION OF BRAIN TUMOR LOCATIONS

Determination of the origin of tumor locations is an important issue in terms of diagnosis and treatment of patients with glioma. The aim of this study was to determine and analyze a probabilistic brain tumor map reflecting tumor observation frequencies in different brain locations. T1-weighted MR images of 232 patients diagnosed with high and low grade brain tumors were analyzed. The data were collected from both online MRI brain tumor data resources shared for academic usage as well as brain tumor patients from Başkent University Hospital. We obtained 78 high and 54 low-grades MRI scans from Başkent University Hospital, and 20 high and 10 low-grades images from the MICCAI 2012 Challenge on Multimodal Brain Tumor Segmentation (BRATS). Combining all these MRI scans together with the use of brain imaging techniques created the probabilistic brain tumor map. Following brain extraction, image registration is implemented to transfer all MRI scans to the reference image coordinates, and individual transformation matrices are obtained for each data. Then brain tumors are segmented, and a radiologist confirmed the segmentation results. Then segmented images are registered to the standard coordinates by multiplying them with their specific transformation matrices.

Our results indicated that there is a difference between high and low-grade tumor regions. Many of tumor positions were around the frontal and temporal ventricular zone for high-grades while the low-grade tumors were located around the posterior ventricular wall. These findings also support the theory that there is a close relationship between gliomas and ventricle region where neural stem cells are emanated.

Keywords: MR, Brain Image Analysis, Registration, Segmentation, Brain Tumor, Glioma, Neural Stem Cell, Probabilistic Map.

ÖZET

BEYİN TUMÖRÜ BÖLGELERİNİN OLASILIKSAL OLARAK BELİRLENMESİ

Beyin tümörlerinin yerlerinin tespiti, tümör hastalarının teşhis ve tedavisi açısından büyük önem arz etmektedir. Bu çalışmanın amacı farklı beyin bölgelerinde tümör görünme sıklığını yansıtan olasılıksal beyin tümörü haritasını oluşturmaktır. Beyin tümörü teşhisi konan toplam 232 hastanın T1 ağırlıklı düşük ve yüksek gradeli MR görüntüleri incelenmiştir. Veriler hem akademik araştırma amacıyla yayınlanan beyin tümörü veri kaynaklarından hem de Başkent Üniversitesi Hastanesi'nin sağladığı beyin tümörü hastalarının verilerinden oluşmaktadır. 78 adet yüksek ve 54 adet düşük gradeli MR verileri Başkent Üniversitesi Hastanesi'nden toplandı. Bunun yanında 20 adet yüksek ve 10 adet düşük gradeli görüntüleri MICCAI 2012 konferansından, 70 adet beyin görüntüsü de REMBRANDT veri tabanından alındı. Beyin tümörü haritası çeşitli görüntüleme yöntemlerinin yardımıyla bütün bu MRI taramalarının birbiri üzerine eklenmesiyle oluşturuldu. Beyin çıkartma yönteminden sonra görüntü çakıştırma yöntemi, bütün MRI taramalarının aynı zeminde değerlendirilmesi için kullanıldı ve her veri için ayrı dönüştürme matrisleri oluşturuldu. Segmente edilen tümörler bu dönüştürme matrisleriyle çarpılarak aynı referans zeminine getirildi.

Elde edilen neticeler gösterdi ki yüksek ve düşük gradeli tümör bölgeleri arasında ufak farklılıklar göze çarpmaktadır. Bir çok beyin tümörü yüksek gradeli verilerde frontal ve temporal ventricular bölgelerde gözlemlenmiş olmasına rağmen düşük gradeli tümörlerde posterior ventricular duvarında olduğu belirlenmiştir. Bu bulgular sinir kök hücrelerinin ortaya çıktığı yerdeki ventricle bölgesi ile beyin tümörü arasında yakın bir ilişki olduğu teorisini desteklemektedir.

Anahtar Sözcükler: MR, beyin tümörü, glioma, beyin görüntü işleme, segmentasyon, çakıştırma, nöral kök hücreleri, olasılıksal harita.

TABLE OF CONTENTS

LIST OF FIGURES

LIST OF TABLES

LIST OF SYMBOLS

A_E	Signal Intensity
B_0	Homogeneous Magnetic Field
M_z^0	Proton Density
B_1	Rotating RF Magnetic Field
T_1	Spin-Lattice Relaxation
T_2	Spin-Spint Intensity
T_E	Echo Time
T_R	Repetition Time

LIST OF ABBREVIATIONS

BRATS	Multimodal Brain Tumor Segmentation
CA	Cellular Automata
CSF	Cerebrospinal Fluid
DTI	Diffusion Tensor Imaging
FMRIB	The Oxford Centre for Functional MRI of the Brain
FSM	Statistical Parametric Mapping
FSL	FMRIB Software Library
MATLAB	MATrix LABoratory
MNI	Montreal Neurological Institute
MRI	Magnetic Resonance Imaging
rCBV	Relative Cerebral Blood Volume
REMBRANDT	The REpository of Molecular BRAin Neoplasia DaTa
RF	Radio Frequency
SVZ	Sub-ventricular Zone

1. INTRODUCTION

1.1 Literature Review and Motivation

In 2014, according to Central Brain Tumor Registry of the United States (CBTRUS), 23,380 people are diagnosed with cancerous brain tumors while 14,320 adults died from the disease in the US. Brain tumors are commonly seen not only in older people but also in the children. 20% of tumor cases observed on children younger than 19. So far, 120 different types of brain tumors were identified. While there is a big effort in detection and treatment of brain tumors, there is also a considerable effort for determining where gliomas are originated. There might be a relation between the location and the place of its origin [1].

Finding the place where brain tumor cell originates is challenging. There are various mathematical models [2] describing glioma growth. Tumor location may give insight about the diagnosis, and brain tumors may have various features comparing the phenotypes of the tumor-based regions [3]. Depending upon where they originate, the tumors may display different progressions [4]. Determination of glioma locations [5] enables to identify the connections between tumor types and the diagnosis as well as to present a different perspective regarding anatomic relations of tumor and its region [6].

Although the source of gliomas has been unnamed, at the present time, the recent studies have revealed that brain tumors may emerged from mutation of neural stem cells that populated in lateral ventricular system walls [7, 8], which is called as sub-ventricular zone (SVZ). SVZ hosts neural stem cells, and plays an important role in self-renewal and reproduction of glial and neurons during a human's lifetime. Both brain tumor cells and neural stem cells have a bunch of typical characters including high motor response and association with blood vessels and white matter tracts [9]; thereby, there is a high probability that gliomas may originate from the neural stem cells resided at SVZ. As a result, the determination of glioma probabilistic map might

provide a contribution to such an approach.

The reason why the segmentation of brain tumors is a highly complicated work is that gliomas do not have a particular shape as of skull, cerebrospinal fluid (CSF) as well as white and grey matter. Hence, specific algorithms are applied to segment gliomas automatically including the comparison of approximate left-right symmetry of a healthy brain [10]. There are also semiautomatic methods used for tumor segmentation. Tumor-cut segmentation introduces a rapid and robust functional tool for tumor detection with minimal user intervention by choosing two points comprising of the longest line covering tumor region [11]. Despite of the appreciable progression in tumor segmentation algorithms, gliomas are preferably detected in manually for it is a more confidential and accurate solution [12]. In this thesis, semi-automatic and manual ways of tumor segmentation methods are utilized according to the type, shape and occupied volume of the brain tumors.

Tumor grades are evaluated as low and high-grade gliomas according to the commonly used magnetic resonance imaging technique (MRI) called as relative cerebral blood volume (rCBV). Hence, low and high-grade gliomas can be evaluated as separately in the determination of a brain's probabilistic tumor map. The difference between the distributions of high and low-grade tumors may help to specify tumor grades; thereby, the determination of original place of tumors can be approximated through such a method [13]. Another aim of this thesis is also the determination of radiation treatment region that is remarkably crucial in reducing the risk of tumor reoccurrence.

We created the probabilistic brain tumor maps through the data obtained from 232 tumor patients including probabilistic brain tumor location by registering and segmenting related structural MRI brain data.

1.2 Gathering MRI Image Data

We had collaborated with Başkent University Hospital. They collected the MRI image data of patients with brain tumor. All MRI data are included of pre-operated T1 and T2 weighted images. We obtained 132 data sets of patients diagnosed with brain tumors. 78 datasets included high-grade glioma patients whereas 54 of them have low-grade gliomas.

We also obtained 20 high, 10 low-grade, and total 30 glioma images from the MICCAI 2012 Challenge on Multimodal Brain Tumor Segmentation (BRATS 2012[1]). Lastly, we gathered 70 MRI datasets of brain tumors from The REpository of Molecular BRAin Neoplasia DaTa (REMBRANDT) project[2] . In total, we had 232 brain tumor patients for the determination of brain tumor probabilistic map to get information about the origin of brain tumors.

1.3 Contribution

In this thesis:

- Brain extraction algorithm is performed in order to remove the skull from MR images.

[1]Brain tumor image data used in this work were obtained from the MICCAI 2012 Challenge on Multimodal Brain Tumor Segmentation (http://www.imm.dtu.dk/projects/BRATS2012) organized by B. Menze, A. Jakab, S. Bauer, M. Reyes, M. Prastawa, and K. Van Leemput. The challenge database contains fully anonymized images from the following institutions: ETH Zurich, University of Bern, University of Debrecen, and University of Utah.

[2]The REpository of Molecular BRAin Neoplasia DaTa (REMBRANDT) project, run by the Glioma Molecular Diagnosis Initiative, is focused on uncovering the underlying causes of glioblastoma multiforme (GBM) cancer. More specifically, the REMBRANDT project seeks to characterize a large number of adult and pediatric primary brain tumors and identify biomarkers by correlating molecular data with extensive retrospective and prospective clinical data. REMBRANDT provides a bioinformatics framework and Web portal that allows researchers to integrate clinical and functional genomics data from clinical trials involving patients suffering from Gliomas. The portal is enabled by caIntegrator and leverages the caBIG Clinical Genomics Object Model (CGOM) to provide Web-based and programmatic access to the data. REMBRANDT currently houses two sets of data: The first comes from the NCI-sponsored Glioma Molecular Diagnostic Initiative, the largest genetic/clinical corollary study ever conducted on Gliomas The second comprises a wide array of molecular and genetic data regarding all types of primary brain tumors.

- All images are registered with the standard-space T1-weighted average structural template image from Montreal Neurological Institute (MNI 152), and are generated separate transformation matrices for each image.
- Tumors are segmented manually or semiautomaticly. Pysicians confirmed the results for the sake of reliability.
- Segmented images are transformed frame of the reference (MNI) brain after they are multiplied with corresponding transformation matrices obtained from registration step.
- All resulting brain segmented images are combined to generate individual brain probabilistic tumor maps as high-grade, low-grade and total image maps of the brain.
- Intensity normalization method is implemented to compare resulting probabilistic maps in the same basis.

The proposed method in this thesis is accepted as a publication by the 37th Annual International Conference of the IEEE Engineering in Medicine and Biology Society (EMBS 2015). Moreover, it is planned to present thesis outcomes in some of the national conferences as 19th Biyomedikal Mühendisliği Ulusal toplantısı (BIYOMUT 2015) and 36th Ulusal Radyoloji Kongresi (TURKRAD 2015). In addition, an article will be submitted to one of the international journals from among American Journal of Roentgenology, European Journal of Radiology, or Magnetic Resonance Materials in Physics, Biology and Medicine.

1.4 Outline

The organization of the thesis is as follows. In Chapter 2, a background on medical image artifacts, difference between low and high-grade gliomas as well as T1 and T2 images, and brain tumors are given with the necessary information to follow the thesis. In Section 3.1 and Section 3.2, brain extraction and registration methods

are described respectively. The proposed segmentation methods in thesis are presented in Section 3.3. Transformation of segmented images and finally the generation of probabilistic brain tumor atlas are mentioned at the rest of Section 3. The results are demonstrated separately depending upon the resources of MRI images in Chapter 4 with deep analysis as well as comparison of high and low-grade results, followed by a conclusion and discussion in Chapter 5.

2. BACKGROUND

In this chapter, used MRI data acquisition methods and glioma features information required to follow the thesis are briefly described. The differences between T1 and T2 images as well as distinctions between low and high-grade brain tumors are presented.

2.1 Image Artifacts in MRI

Although MRI imaging technique is widely used by physicians and researchers, gliomas are hardly eliminated due to the acquired signal intensity that in some cases greatly reduces the image quality. These artifacts can be classified as three categories.

- Main magnetic field distortion caused by the inhomogeneity in homogeneous magnetic field (B_0). It may result in the image distortions as spatial or intensity distortions, or both [14].
- Gradient field artifacts due to the improper function of the gradient field coils bring about the inhomogeneity along the gradient direction or the abnormal current passing through the coils [15].
- Radio frequency (RF) inhomogeneity, called as bias field, result from either a non-uniform rotating RF magnetic field (B_1) or a non-uniform sensitivity in receiving only coil [16].

MRI pre-processing imaging techniques are extremely crucial implementations to cope with such distortions in the determination of high quality data, so as accurate diagnosis of illness. Even though some of the solutions to MRI artifacts are applied during the process of MRI test, additional corrections on images should be performed on acquired MRI data to increase the performance of the post processing applications.

Hence, we will concentrate on choosing the most appropriate parameters and methods during the brain extraction, registration and segmentation processes.

2.2 Brain Tumors & Low and High Grade Gliomas

According to the MRI data, the diagnosis is identified whether the glioma is benign or malign. The radiologist checks bleeding and necrosis around the tumor and observes invasive effects on neighborhood structures. Consequently, tumor pathology is diagnosed to decide on the treatment type.

Some tumors arise elsewhere in the body and metastasized to the brain whereas some are originated in the brain. These glioma types are called as secondary and primary brain tumors respectively. Glia cells function as supportive structure to the brain and serve nerve cells in their activity as maintaining fundamental nutrition and appropriate water ion concentration. Glia cell mutation is the main source of primary brain tumors. Gliomas are classified into four grades as grade I, II, III and IV. Grade I and II tumors are named as low-grade gliomas whereas grade III and IV tumors are high-grades. After the determination of which class the glioma fits, the treatment and prognosis are preceded accordingly [17].

Low-grade gliomas are categorized in terms of the tumor appearance as diffuse and pilocytic astrocytomas, oligodendrogliomas, gangliogliomas, and mixed gliomas. Patients diagnosed with any type of low-grade gliomas mostly do not need any surgical operation. These types of tumors are benign tumors and localized narrowly. They generally do not spread outside the brain and do not increase in size. Since low-grade gliomas hold a small amount of contrast during the data acquisition process, they have more homogeneous images as shown in Figure 2.1.

High-grade gliomas, which are roughly malignant tumors, are classified into two groups as Grade 3 that includes astrocytoma, oligoastrocytoma and ependymoma, and as Grade 4 that only includes glioblastoma. Gliomas grow inside the brain region and

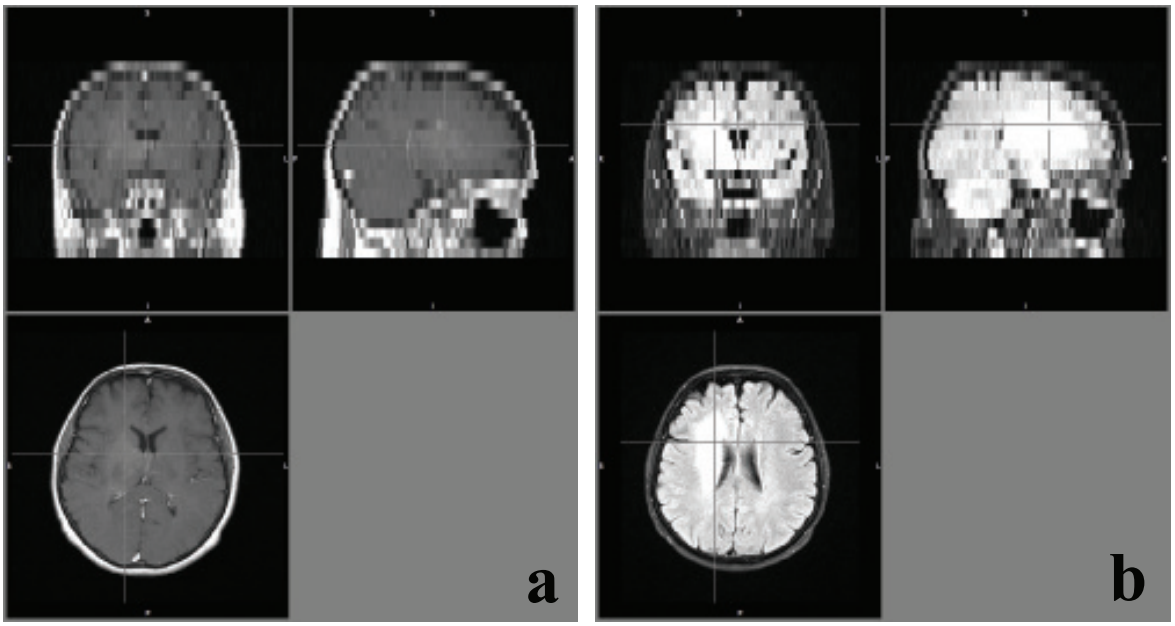

Figure 2.1 Low grade glioma MRI data including T1 (a) and T2 (b) images.

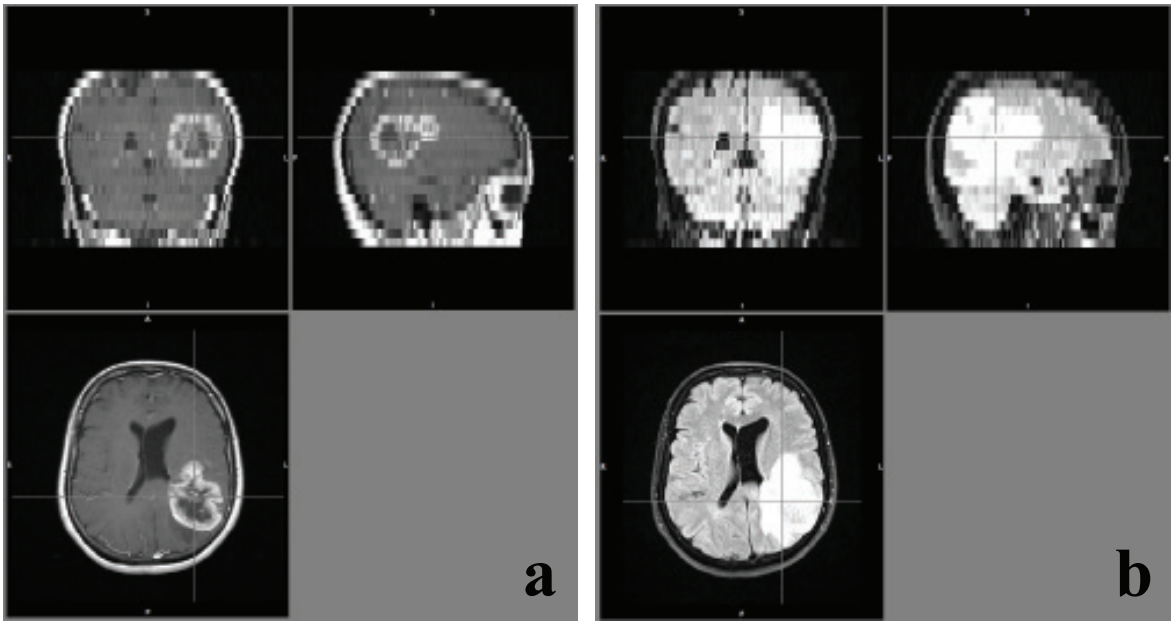

Figure 2.2 High grade glioma MRI data including T1 (a) and T2 (b) images.

makes pressure in nearby normal brain tissue. Since such gliomas have vital adverse effects on the brain functioning, patients are subjected to surgical operation for the treatment. As it can be observed from the Figure 2.2, high-grade gliomas can be observed explicitly because of the necrotic areas.

To sum up, it is easier to segment high-grade tumors than low-grades because of the contrast differences in MRI data. Both high and low-grade brain tumors can be observed with the use of T1 weighted images. On the other hand, some of low-grade images are better detected on T2 images, which will be explained later on.

2.3 T1 and T2 Images

T1 relaxation constitutes for the time constant determining the rate of longitudinal magnetization along the (z) axis following an RF pulse. During the process of T2 relaxation, transverse magnetization along the (xy) plane following excitation results in permanent loss in magnetization. T1 relaxation is also called as spin-lattice relaxation while T2 refers to the spin-spin relaxation time [18].

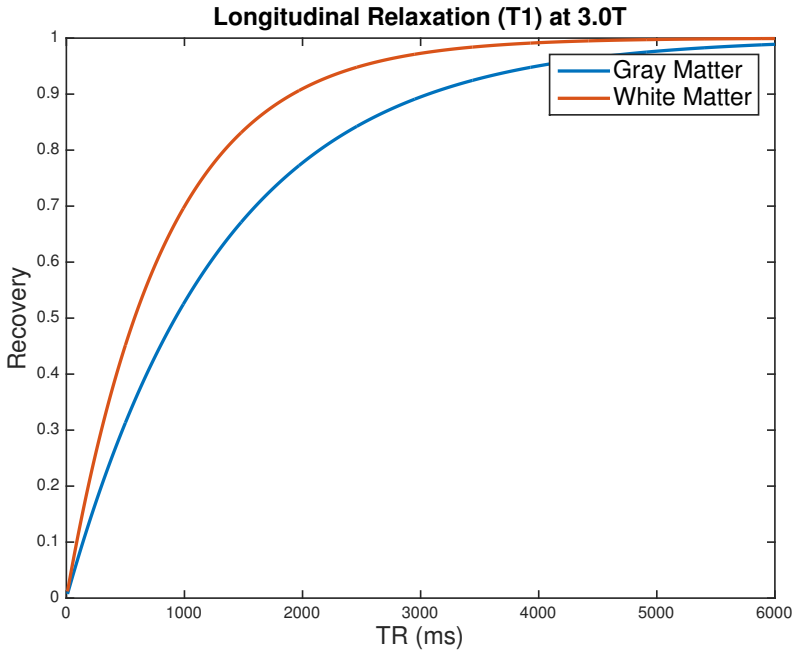

Figure 2.3 T1 relaxation characteristic curve.

Calculation of T1 and T2 values for brain tissues requires the acquisition of images at different imaging parameters. Signal intensity for spin-echo relaxation can be expressed as;

$$A_E = M_z^0(1 - e^{-T_R/T_1})e^{-T_E/T_2} \tag{2.1}$$

where A_E is the signal intensity acquired, M_z^0 is the proton density, T_R is the repetition time and T_E is the echo time.

T1-weighted MR image is calculated by choosing a short echo time (T_E) to get rid of T_2 effect on the images. Then, the signal intensity reduces to the following equation 2.2. As a result, the exponentially increasing curve in Figure 2.3 can be sampled by changing repetition time.

$$A_E = M_z^0(1 - e^{-T_R/T_1}) \tag{2.2}$$

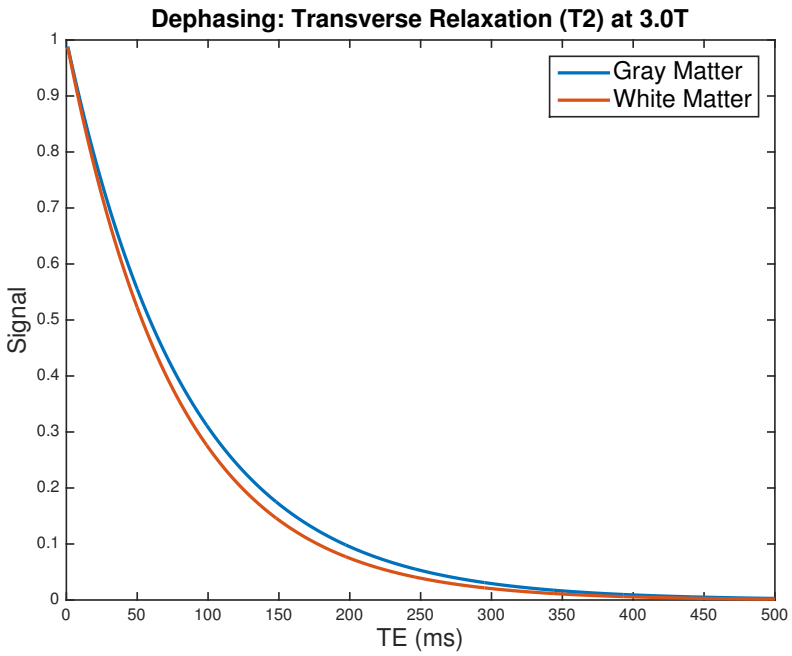

Figure 2.4 T2 relaxation characteristic curve.

In comparison with the T1-weighted image procedure, T2-weighted MR data is gathered by taking long T_R relative to the T_1 values of the tissues in order to remove T_1 the effect. The signal intensity A_E goes up exponentially according to the equation

2.3.

$$A_E = M_z^0 e^{-T_E/T_2} \tag{2.3}$$

As clearly explained by former equations and graphs in this section, there is a distinction between the acquired T1 and T2 weighted MRI images. Since high-grade tumors hold the contrast better, gliomas are observed clearly in T1 data. Conversely, T2 data includes the detection of low-grade gliomas with higher quality. As a result, both T1 and T2 weighted MRI images will be employed to compose low and high-grade probabilistic tumor maps.

3. METHODS

In order to obtain a probabilistic map of tumors on the brain, MRI images are preprocessed for brain extraction, registration, and tumor segmentation and transformation with the use of particular medical imaging tools.

3.1 MRI Image Analysis Tools

MRI is vulnerable to the magnetic field changes due to the applied radio frequency pulses in the presence of magnetic field gradients. Hence, MRI imaging process is sensitive to disturbances such as scanning room conditions or imperfect alignment of MRI machine. A number of imaging software programs are commonly used in order to remove these effects. In this study, we used quite a few complicated imaging tools including filtering, brain extraction, image registration, and segmentation, when insufficient, manual ways are also utilized to analyze such individual situations.

FSL [19–21], SPM [22], and ITK-SNAP [23] are all broadly used tools in medical image processing. ITK- SNAP program is very advanced in 3D visualization and manual segmentation of scanned images. Moreover, SPM is composed of a set of MATLAB functions as well as user-friendly interface. It is easy to use but runs slowly due to the restrictions of MATLAB. On the other hand, FSL can operate in Ubuntu/Linux; thereby, user may prefer using Linux Terminal to run FSL codes by writing batch codes for the automatic analysis of huge numbers of MRI images in one click. In this study, semi automatic segmentation is applied to particular images using a specific tool named as Tumor-cut Program [11], which is coded through MATLAB. On the other hand, manual segmentation using ITK-SNAP is implemented in most cases for the reliability of segmenting tumors. Furthermore, a radiologist validates all the segmented images.

3.2 Brain Extraction (BET)

MRI gives the image of the whole head including skull and the brain. In order not to mislead preprocessing methods, especially for the segmentation process, it is crucial to pick up only the brain image of the patient.

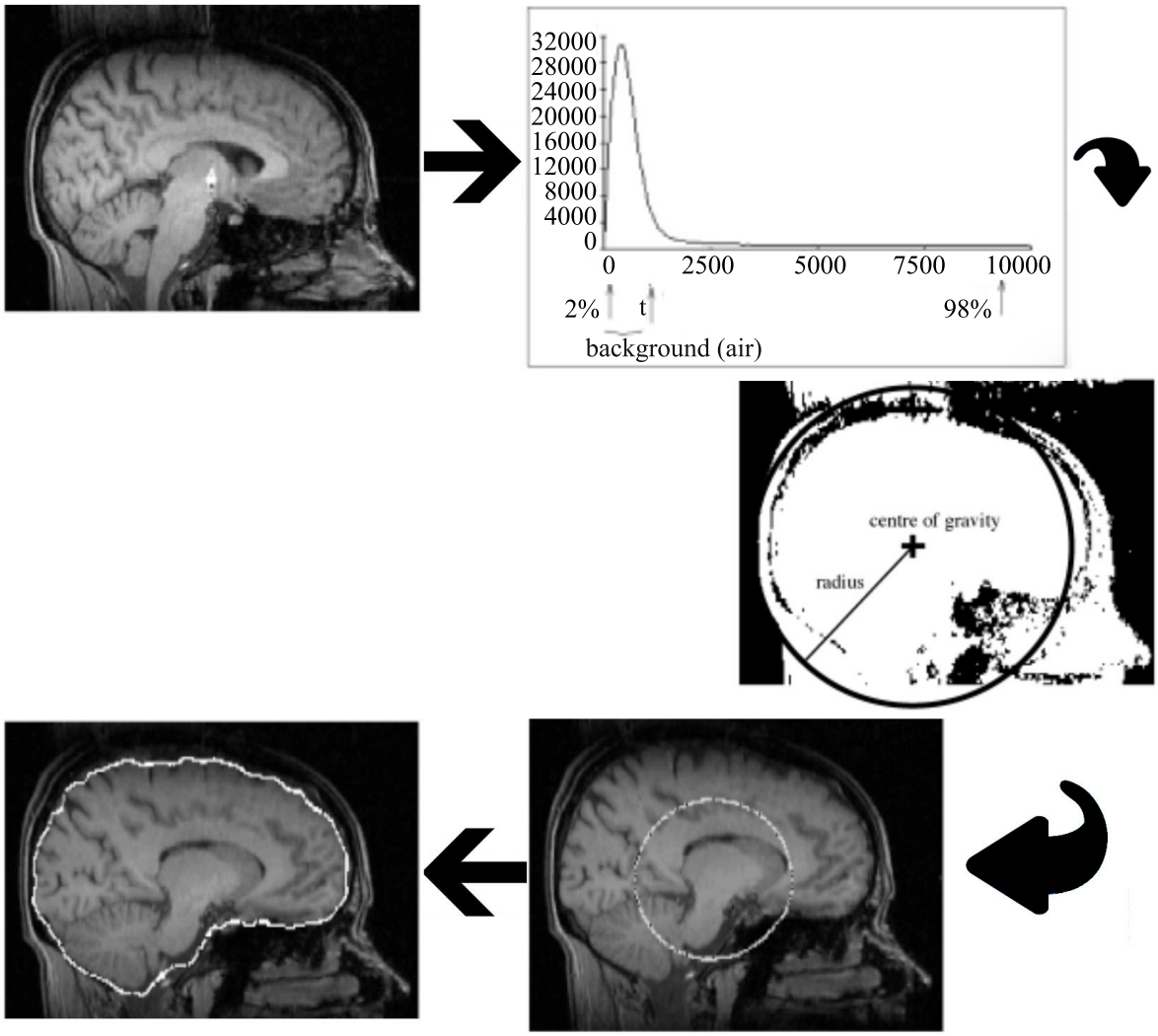

Figure 3.1 BET processing flowchart

FSL is employed for its effective toolbox for brain extraction [24]. BET tool first brings about the intensity histogram from the MRI image to determine "robust" lower and upper intensity values. According to histogram thresholds, it separates brain tissue from the non-brain tissue roughly. Furthermore, rough size and the center of mass of the head are acquired. A triangular tessellation of a sphere's surface is set

up on the center of mass of the brain and it starts distortion of one vertex at a time gradually by following forces that keep the surface well spaced and smooth. In this way, the algorithm tries to determine the contacting regions of the brain and the skull, that is to say the edge of the brain tissue. If a pleasantly bright edge is not resolved, a higher smoothness constraint is chosen and this process reruns to reach a pleasant solution. At the end, the outer region of the skull is measured if needed. As a result, the neighboring line between brain and skull is determined considering such features and the skull is stripped [24]. The graphical schematic of the process is given in Figure 3.1.

Boundary around the brain is stripped with the use of BET tool, and only the brain volume is left for further processing. Fractional intensity threshold (FIT) is defined as the threshold level between brain and other head structures. It takes values in between 0 and 1. If it is close to zero, it means more brain volume is left out. FIT is chosen by trial and error as 0.4, which is defined as the optimum value.

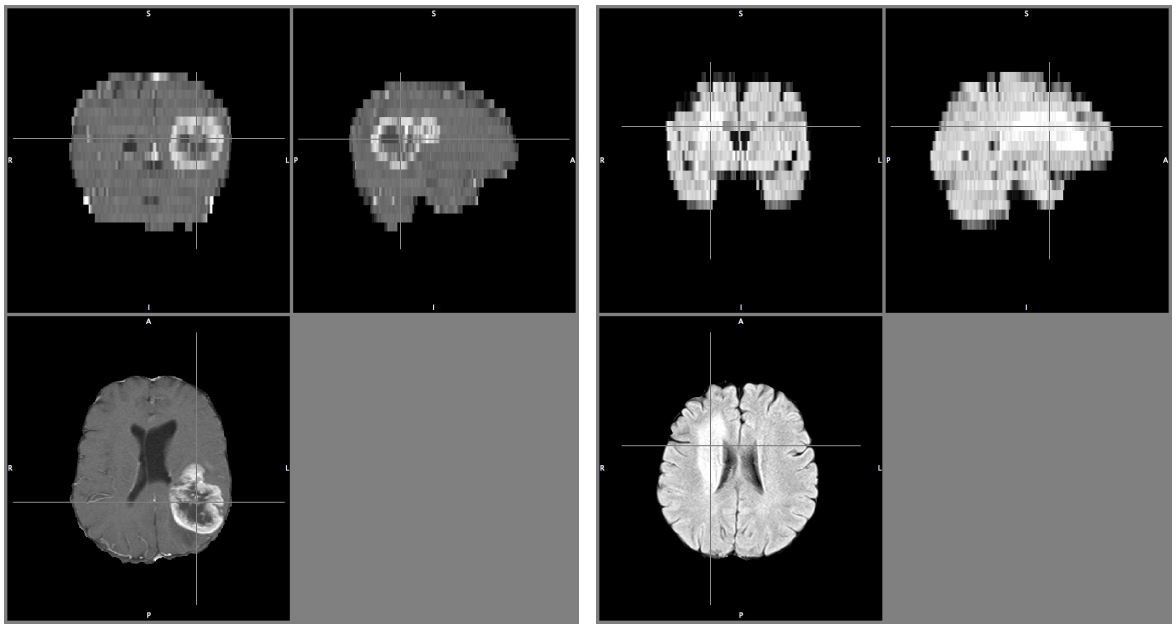

Figure 3.2 BET result of both high and low glioma images

3.3 Image Registration

Mathematically, the registration problem is an estimation of a transformation matrix between a moving image $I_1(X)$ and a reference image $I_2(X)$. In this way, the moving image is transferred into the coordinate system of the reference image by the use of estimated transformation matrix. Hence, the similarity measure can be represented as $S(I_1(X), I_2(T(X)))$.

Registration methods can be classified as linear (rigid or affine) or deformable. In this study we only needed linear methods. Rigid transformation is mainly composed of the translation and the rotation of the image coordinates to the basis image. On the other hand, affine transformation includes more aspects than rigid transformation like scaling and shearing as well as rigid constraints. In short, affine transformation performs better and more accurate registration method in than rigid registration.

In addition to rigid and affine transformations, parametric registration constructs a finite number of transformation matrix parameters by achieving maximum similarity between the reference and the registered image. 3D image has three dimensions such that rigid mapping requires 3 rotation and 3 translation (totally 6) parameters while affine transform requires 3 scales and 3 shear (totally 12 degrees of freedom) parameters. Estimation of these parameters is a cumbersome process, which is hotly debated research area among medical imaging community [25].

$$\begin{bmatrix} x \\ y \\ z \\ 1 \end{bmatrix} = \begin{bmatrix} \alpha_{11} & \alpha_{12} & \alpha_{13} & t_x \\ \alpha_{21} & \alpha_{22} & \alpha_{23} & t_y \\ \alpha_{31} & \alpha_{32} & \alpha_{33} & t_z \\ 0 & 0 & 0 & 1 \end{bmatrix} \begin{bmatrix} x' \\ y' \\ z' \\ 1 \end{bmatrix} \tag{3.1}$$

If needed, non-linear methods of registration are generally implemented after linear registration. A popular approach to linear (affine) analysis is the generation

of mapping function Ω. The elements of Ω stand for a product of a transformation matrix T with homogeneous coordinates in the original image. A sample mapping is shown below formula where $[x\ y\ z]^T$ and $[x^{'}\ y^{\prime}\ z^{\prime}]^T$ represent homogeneous coordinates of reference and moving images respectively [26].

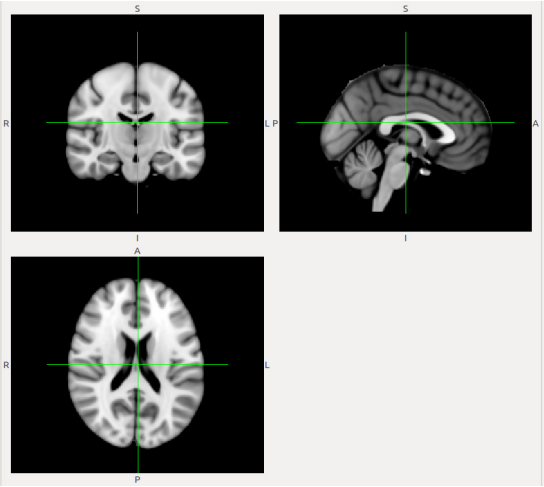

Figure 3.3 MNI152 standard-space T1-weighted average structural template image

All MRI images should be transformed to a template (reference) image to be evaluated them in the same basis. Moreover, we obtained appropriate spatial transformation matrices after image registration, and used them to convert segmented images to a reference coordinate system.

Medical imaging tools like FSL [27, 28] present users to implement registration in different degrees of freedom as 6, 7, 9, 12 degrees. Moreover, it has different interpolation methods as nearest neighbor, sinc, and spline methods. It also includes a variety of cost functions that can be categorized as least squares, normalized correlation, as well as correlation ratio. Among these, sinc and least square with 12 degrees of freedom gave the best registration consistently.

We extracted the brain tissue, and the result was shown on Figure 3.2. As an example presentation, the registration result of these images can be seen on Figure 3.4.

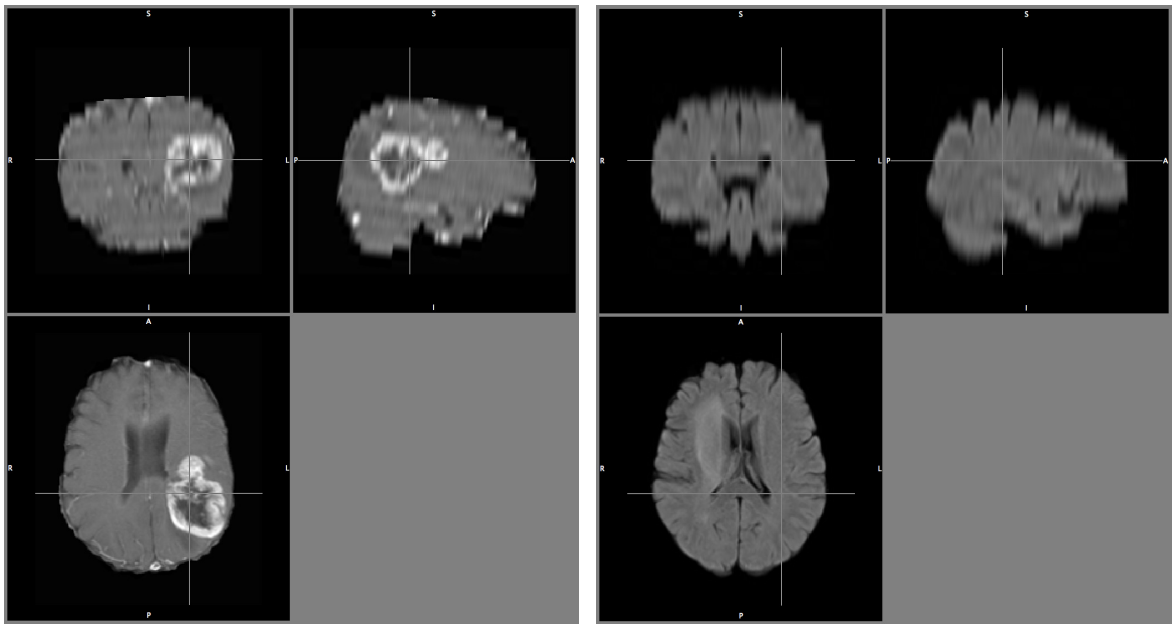

Figure 3.4 Registration result of both high and low glioma images

3.4 Tumor Segmentation

On the brain studies, segmentation is frequently used FSL tool to differentiate separate parts of the brain, i.e. CSF, gray or white matter and tumor/edema. Moreover, physicians have been detecting the tumor region with reference to their experience and intuition. On the other hand, especially in recent years, automatic tumor segmentation methods became popular to detect the tumor regions in brain in a quantitative way [29].

Perfusion, diffusion or spectroscopic imaging techniques give unclear results in tumor segmentation due to their low resolution compared to conventional MRI. While some algorithms utilize the differences in T1 weighted and post contrast T1 weighted images, T2 weighted images are also used for the detection of non observable elements in T1 data. In this study, we utilized post contrast T1 weighted images successfully. Despite the appreciable progress in automatic tumor segmentation algorithms, the segmentation of MRI brain images is still a challenging process due to various disturbances and artifacts. Therefore, we still needed to operate manual segmentations checked by radiologists to establish a ground truth.

3.4.1 Semi-automatic Tumor Segmentation

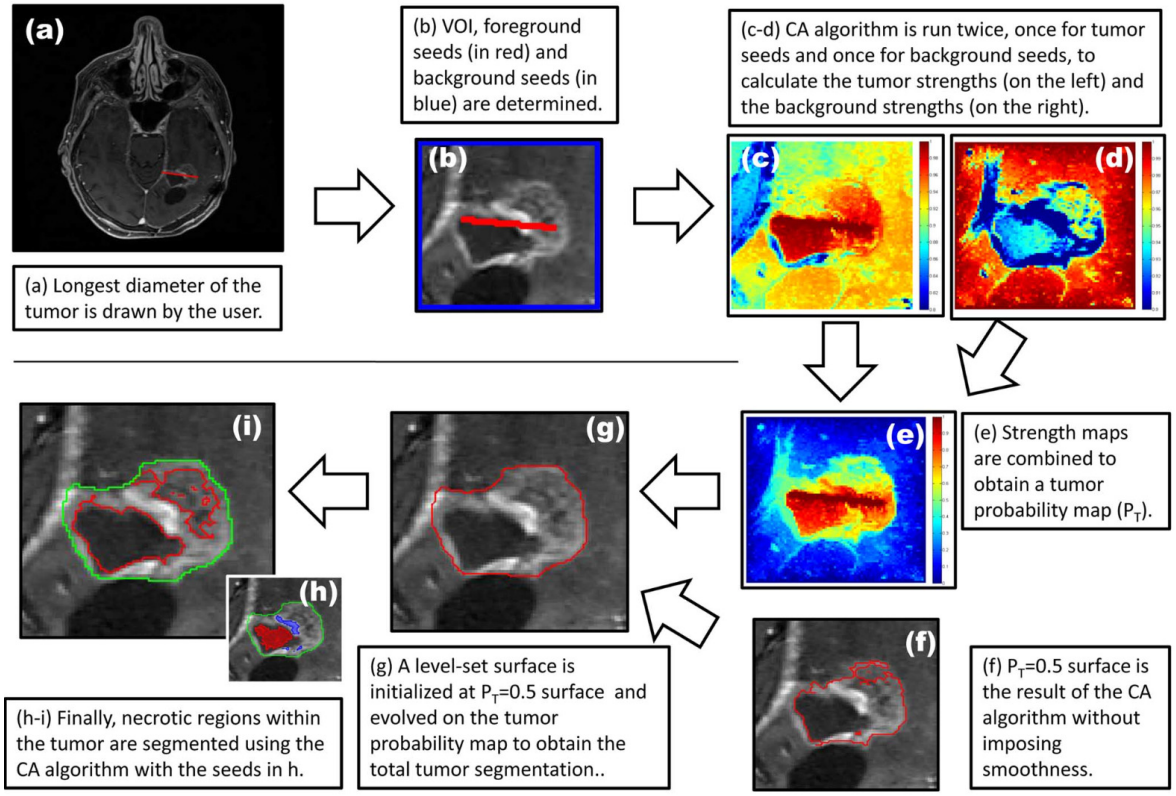

Figure 3.5 Steps of the proposed tumor segmentation method[11].

Tumor-cut algorithm, which is developed by Andaç Hamamcı [11], is used to segment brain tumors from the brain tissue in a semi-automatic way. The method is semi-automatic, requiring the user to draw the maximum diameter of the tumor, which takes about a minute user-interaction time per case. The typical run-time for each case is around 10-20 minutes depending on the size of the tumor. Steps of the proposed cellular automata (CA) based tumor segmentation algorithm is shown in 3.1 First, (a) the user draws a line over the largest visible diameter of the tumor; (b) using this line, a VOI is selected with foreground (red)-background (blue) seeds; (c)&(d) tumor CA algorithm is run on the VOI for each two sets of seeds (for the foreground and background) to obtain strength maps for foreground (c) and background (d) at each voxel; (e) two strength maps are combined to obtain the tumor probability map (6); (f) a level set surface is initialized at $P_T = 0.5$ is used to evolve the surface which converges to the final segmentation map (g). Finally, (i) the necrotic regions of the

tumor are segmented using a CA-based method with the chosen enhanced and necrotic seeds in (h).

This algorithm gives advanced result in highly qualified T1-C images including small size tumors. It also differentiates the edema regions around tumors. The MRI images regarding T1-weighted high-grade tumors give clear segmentation results due to composing of the distinct intensities between tumor and brain tissue with the help of injected contrast agents to patients. On the other hand, since low-grade gliomas do not hold contrast agent properly in T1 weighted scans, tumor-cut algorithm generally fails in the detection of tumor regions.

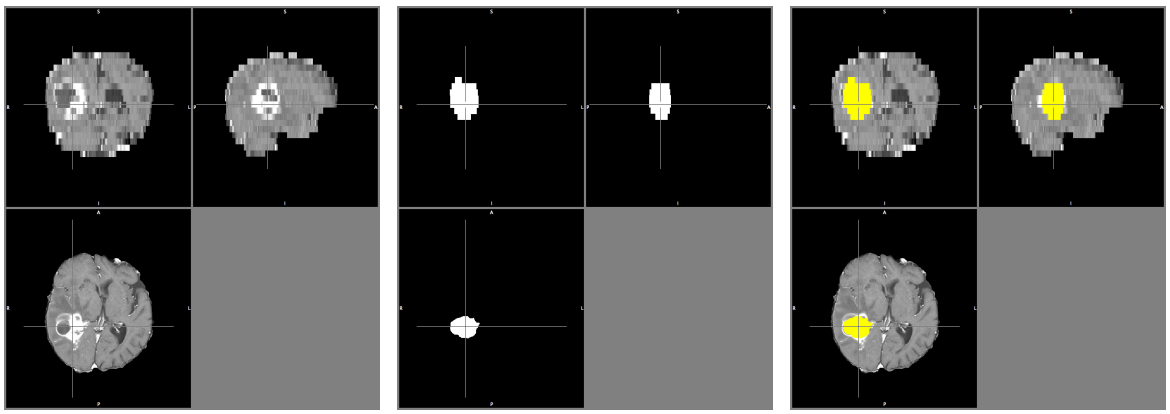

Figure 3.6 Tumor-cut brain tumor segmentation example of a high grade glioma image

3.4.2 Manual Segmentation

Tumor-cut algorithm takes about less than 60 seconds to obtain segmented MRI data for small size gliomas while the algorithm needs to operate for a time period more than 10 minutes to obtain the tumor regions for larger size gliomas. Since I have 232 datasets, I would need to wait approximately 40 hours to observe all resulting segmented images. Moreover, not all acquired segmentation results identify the accurate tumor regions. Therefore, I preferred to use manual tumor segmentation ways for MRI data including high size gliomas of high-grades and including all low-grade tumors with the use of ITK-SNAP segmentation tool.

In ITK-SNAP tool, we can determine a label for brain tumors as a number of 255, which stands for the full white region. When the MRI image is loaded to SNAP, slice-by-slice segmentation can be initiated by drawing a line around the tumor region for each slice. Then, SNAP makes the segmentation in all three orthogonal slice windows by labeling tumor regions as full white, and others as full black.

3.4.3 Tumor Segmentation of Particular T2-Weighted Images

In some cases, especially for low-grade gliomas, tumor regions are not able to be detected even using manual ways in T1-weighted images. As shown in the figure below, which is of the brain of a patient with low-grade glioma from Başkent University, glioma region is not observed in T1-weighted image. Hence, we should utilize from another type of MRI data, which is accused of T2-weighted MRI scan.

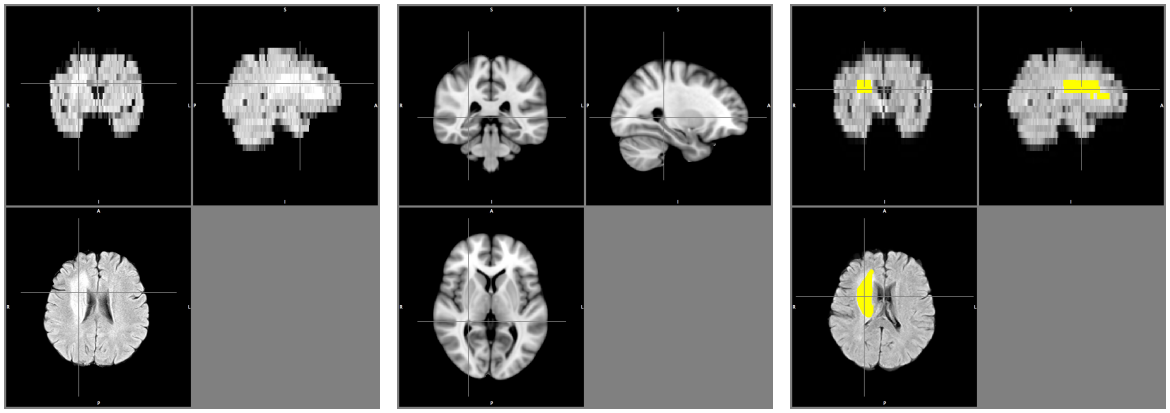

Figure 3.7 Particular T2-weighted images are first converted to T1 reference plain, and then subjected of segmentation process.

The standard protocol used in observing tumor regions by physicians is investigation of both T1 and T2 weighted MRI scans according to the glioma type during the diagnosis process. At this stage, there are particular findings to determine whether tumor type is benign or malign. They also look around tumor regions in terms of blood or nechrosis originated. At the end, physicians determine the tumor type as low or high-grade glioma.

Because high-grade gliomas carry nechrosis-center feature, they hold contrast agent better; thereby, they are explicitly seen on T1-weighted contrast data. On the other hand, low-grade glioma image exhibits more homogenous characteristic with regards to signal intensity differences. That's why we could not detect tumor regions in some of the cases in T1-weighted images. On the other side, gliomas were clearly observed in T2-weighted data of the same patients. Hence, we did the registration of T2-weighted images onto their T1 weighted data, and applied the manual tumor segmentation accordingly.

3.4.4 Transformation of Segmented Images

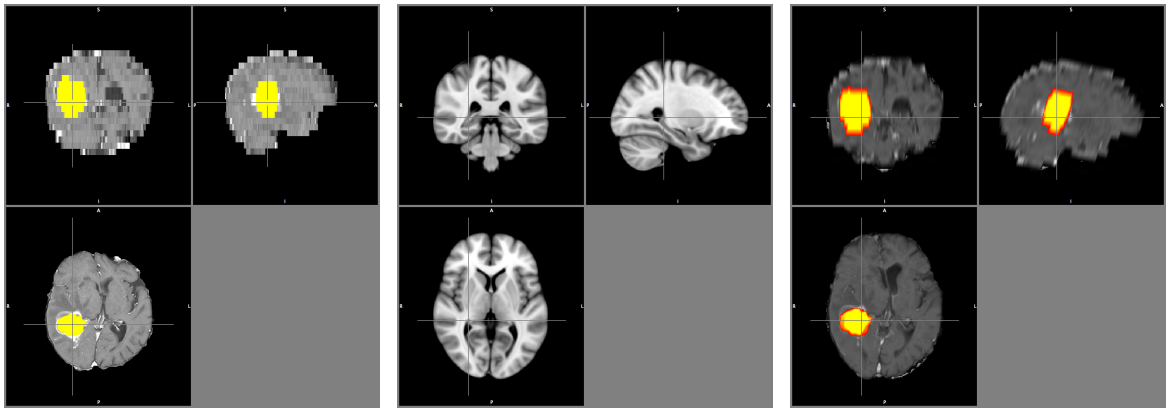

Figure 3.8 Transformation of segmented images to the reference plane (MNI template).

Until now, all data used in this work are registered to MNI 152 space as a reference brain map. On the other side, tumors in all images are segmented, and a radiologist as a ground truth checks segmented tumors. Then, all glioma-segmented images should be transformed to evaluate the size and the place of tumors in the same basis. After the brain image registration, we obtained individual transformation matrices for each MRI data. When tumor segmented images are multiplied with their specific transformation matrices, they become transmitted to the MNI 152 reference brain map. Therefore, we get ready to add them together to obtain a probabilistic brain tumor map.

3.5 Probabilistic Brain Tumor Map

There are variety of technical issues in generation of probabilistic tumor map. At first, the brain volumes were extracted from acquired MRI data. Next, skull stripped structural MRI data were registered with respect to the reference brain image volume from Montreal Neurological Institute (MNI 152) [30,31]. As a result of the registration, transformation matrices for each MRI data obtained. Tumor tissues in brain images are segmented. All segmentation results were reviewed and segmented manually when needed. A physician confirms segmentation results. Afterwards, the tumor tissues are registered by using the transformation matrices that were acquired during the registration process. As a result, each tumor data from different patients are mapped to a standard brain atlas; thereby, we attained a probabilistic map of brain tumors and evaluated the resulting images. During this process, we employed two image processing tools; FSL and ITK-SNAP.

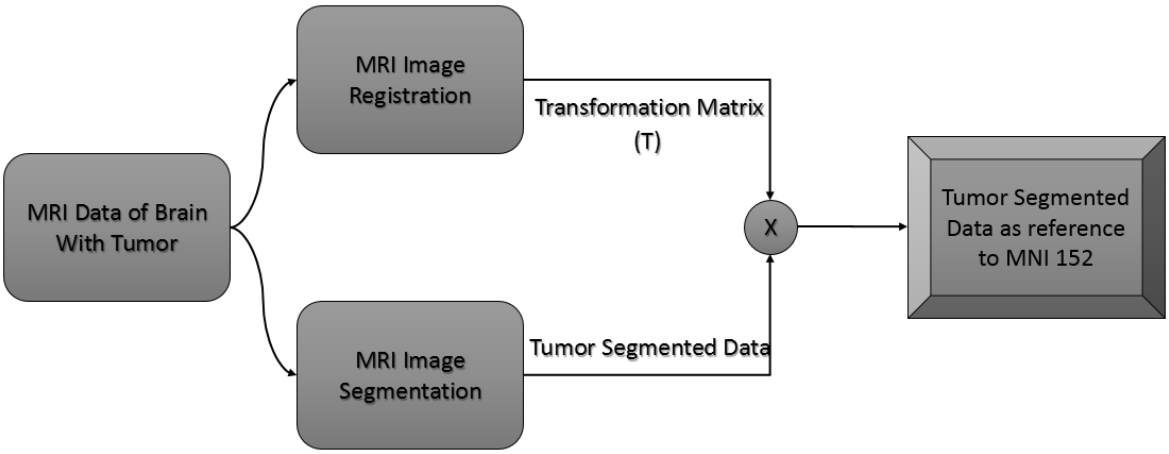

Figure 3.9 Probabilistic brain tumor map generation steps. MRI data first gets into both registration and segmentation processes, and the resulting transformation matrix from registration is used bringing segmented MRI data to MNI 152 reference. This analysis is done for all patients MRI data and results are added together to compose a probabilistic tumor map.

3.6 Differentiation of Glioma Types Using Probabilistic Brain Tumor Maps

The prediction of glioma types is a cumbersome process because of irregular alignment of brain tumors. Physicians decide glioma grades by observing tissue bleeding or propagation throughout the brain tissue. As a consequence, we might contribute the detection of glioma types comparing the correlation between the high and low grade probabilistic brain tumor maps.

3.6.1 Dot Product Comparison

10 images of both high and low grade brain tumor segmented data from Başkent University are randomly chosen for each iteration as testing data. The rest of data from Başkent University are treated to generate high-grade and low-grade probabilistic maps. Then, we applied dot product between each test data with high grade and low grade glioma maps respectively. Since we know the image type, we compared the result of high grade test data dot product by high grade and low grade maps as well as vice verse for low grade test data. If the resulting value from high grade map multiplication is higher for high grade test images, it means that the algorithm meet to the target, we counted for how many high grade test images the algorithms succeeds. We applied the same methodology to the low grade test images, and counted the success rate of the algorithm. We also aimed to normalize the dot product comparison results. For this purpose, we divided each dot product results to the value obtained by the addition of each voxels including total area between test image and glioma maps.

3.6.2 Center of Mass Comparison

We recognized a distinction between high and low-grade glioma maps including their centers of masses. That's why we aimed to measure the distinction between center-of-mass of glioma maps and test images. We implemented the same methodology in the

process of randomly chosen test data and generation of probabilistic maps. For each high-grade test images, we calculated their center-of-mass, and measured the distance to the center-of-mass of high grade and low grade brain tumor probabilistic maps. For each high-grade test data, if its center-of-mass is close to the center-of-mass of high grade glioma map, we accepted that the algorithm predicted the glioma type truly, and we counted for how many test images the algorithm hit the target. Total opposite procedure is applied for the determination of success rate of low-grade test images.

3.6.3 K-means Clustering Comparison of Gliomas

We also implemented k-means clustering algorithm to the dataset from Başkent University. We did the same procedure in obtaining probabilistic glioma maps and randomly selection of test images. We created a 2*n matrix which holds resulting values of high and low grade dot products by high and low-grade glioma maps. Afterwards, we created 2 clusters from this matrix with the use of k-means clustering algorithm by MATLAB. The algorithm divides all observations into two groups, and the division line is accounted for the differentiation region of high and low-grade test images.

3.6.4 White and Gray Matter Registration of Glioma Maps

Till now, we only utilized from the resulting probabilistic brain tumor maps. When the maps are deeply examined, the tumours are observed close to the white and gray matter tracts. Therefore, we registered glioma maps to the gray and white matter segmented MNI 152 template. Then, we applied the method mentioned in the first procedure to the resulting maps to have an idea about the relation between tumors and the brain tracts.

4. RESULTS

In this work, structural MRI data of tumor patients and the grades of resulting tumors are combined together. The main purpose of this study was to obtain a probabilistic tumor map of the brain that helps to determine where tumors on the brain are emanated. Hence, tumors are differentiated with locational relevance with respect to a reference brain map, which was chosen as MNI 152.

We analyzed MRI scans of 232 patients with tumors. Pre-treatment MRI data of brain tumor patients collected and analyzed using advanced imaging techniques. 20 high, 10 low-grade, and total 30 images were acquired from BRATS 2012. Furthermore, 78 high, 54 low-grade, and total 132 images were obtained from Başkent University Hospital. We gathered 70 MRI images with brain tumors from REMBRANDT.

Note that the maximum and minimum signal intensity threshold is shown on the image in the following resulting images of probabilistic brain tumor maps. To make it clear, minimum threshold serves as a means to display the minimum value under which the tumor regions are not presented. Furthermore, it gets more yellow if tumor-observing rate gets higher. The region will turn to a more reddish tone, as tumors get rare as a visualization of probabilistic maps.

In addition to the signal intensity, we normalized all resulting images to evaluate them in the same basis. 12 patients across 132 Başkent University patients with glioma are recognized to have brain tumors in the same region of interest. Hence, we determined approximately the value of 9% (12/132) as a normalization constant. To put it another way, threshold levels were taken between $0.09 * x$ and $2/3 * 0.09x$ where x is the total number of images in a dataset. For instance, the highest threshold value for 132 images is determined as $0.09 * 132 \approx 12$ while the lowest is $2/3 * 0.09 * 132 \approx 8$, which shows that tumor observing rates greater than 8 will turn to red & yellow intensity tones. Table 4.1 presents all data threshold levels for each data sources comparatively.

Table 4.1
Probabilistic brain tumor maps comparison chart. All figures are generated according to the values presented in this table. (LHG stands for low and high grade gliomas while LG is low grade and HG is high grade.)

Data Resource	Data Type	Number of Images	Maximum Threshold	Minimum Threshold
Başkent University	HG	78	7	5
	LG	54	5	3
	LHG	132	12	8
BRATS	HG	20	1,8	1
	LG	10	0,9	1
	LHG	30	2,7	2
Başkent University & BRATS	HG	98	9	6
	LG	64	6	4
	LHG	162	15	10
REMBRANDT		70	7	5
Başkent University & REMBRANDT		202	19	13
TOTAL		232	22	14

The last but not the least important note is that we are studying with a 3D image data, but visualizing them in 2D throughout the thesis. Hence, we tried to exhibit resulting probabilistic brain tumor maps as the most properly observable as possible. Notwithstanding we did show the best results, the reader must remember the dataset being 3 dimensional.

4.1 Probabilistic Brain Tumor Map of Başkent University Hospital Dataset

We obtained brain probabilistic brain tumor map for both high-grade and low-grade images from Başkent University Hospital separately. Figure 4.1 shows the pixel-wise addition of tumor regions on the template brain (MNI 152) comprising of 78 high-grade MRI images. Note that threshold level is calculated 5 as minimum and 7 as maximum intensity level. High-grade tumors are existed commonly around superior and nearly right lateral ventricle zone. Contrary to the high-grade map, gliomas

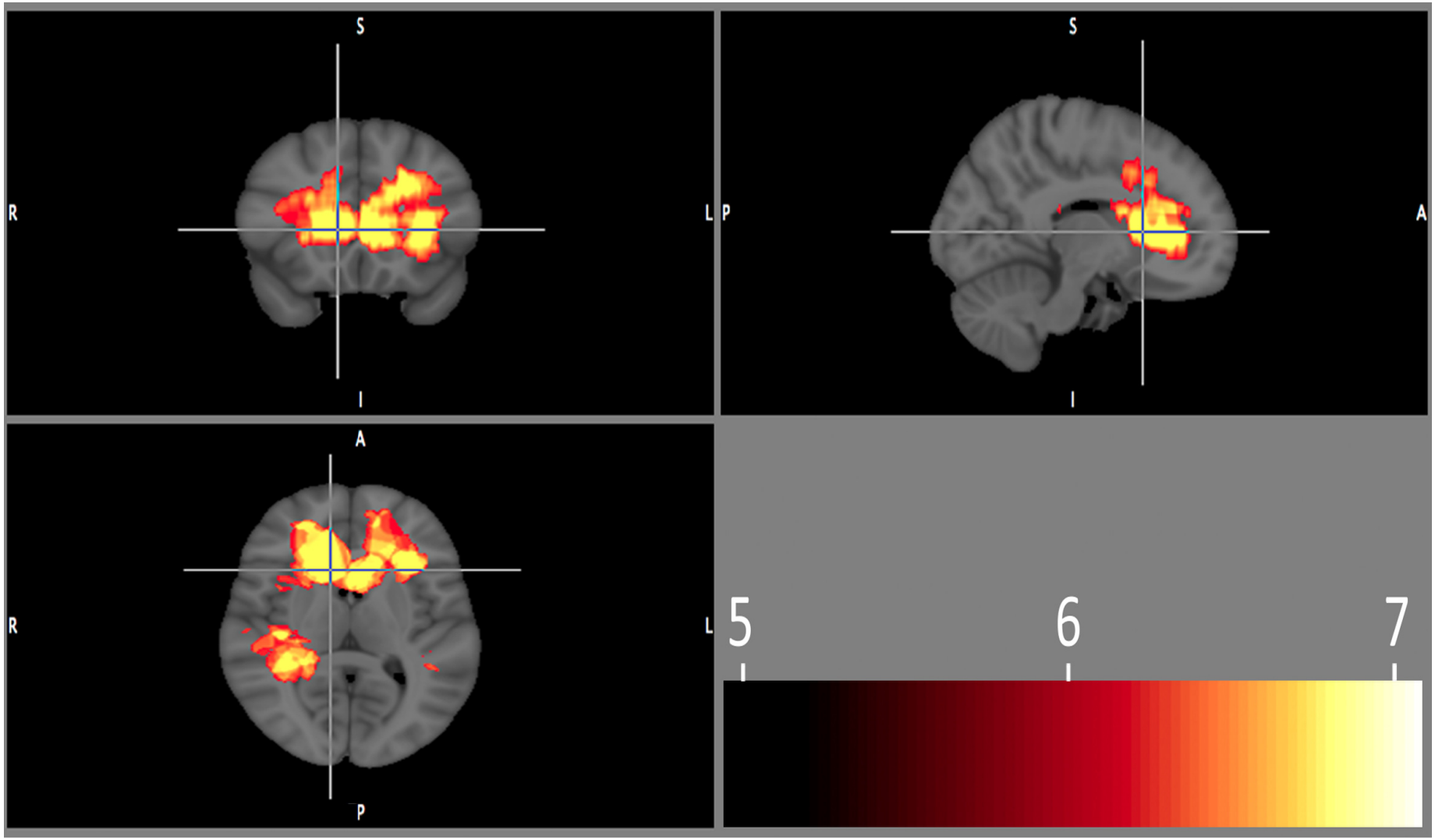

Figure 4.1 Probabilistic brain tumor map of 78 high grade gliomas from Başkent University patients

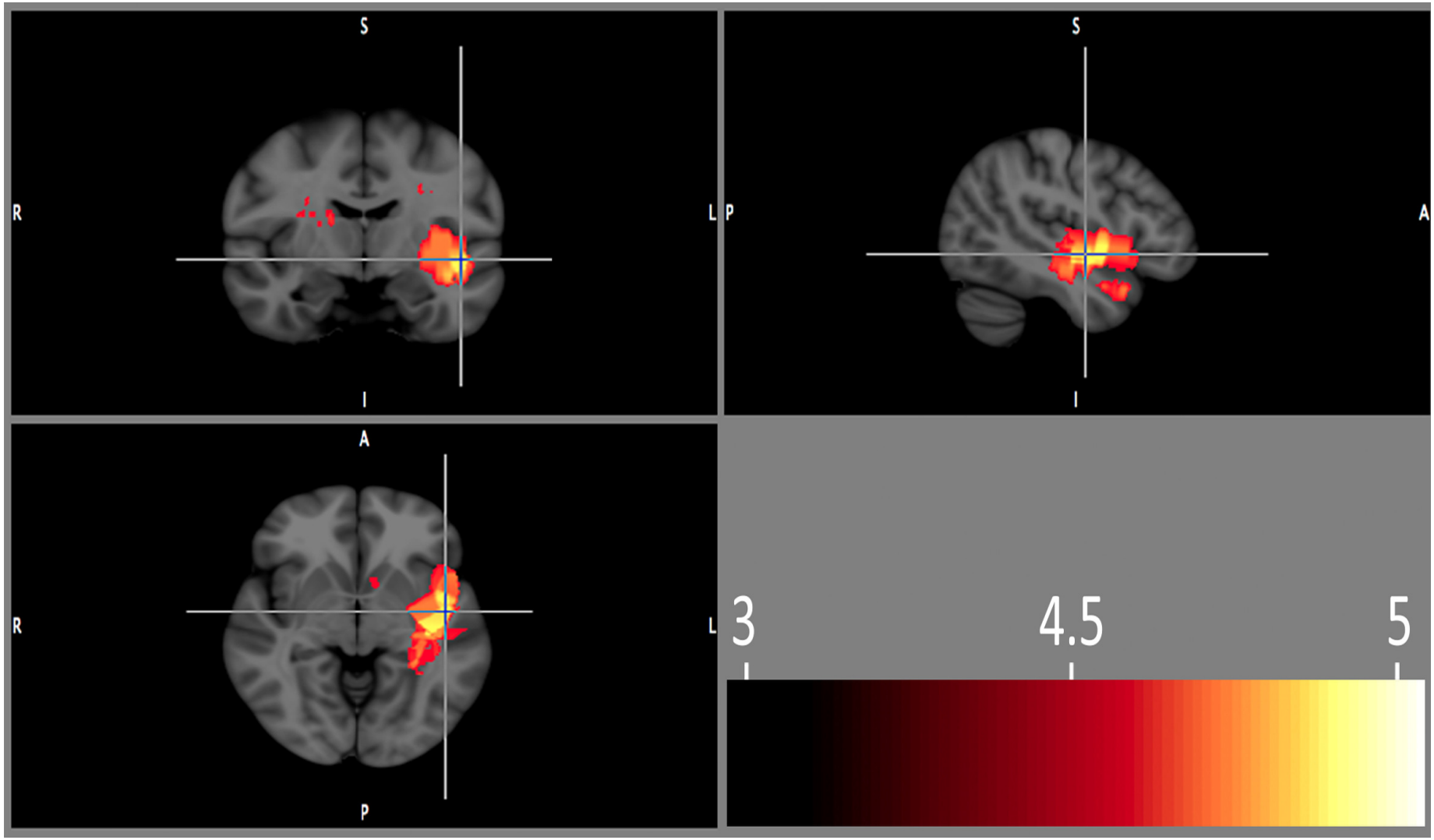

Figure 4.2 Probabilistic brain tumor map of 54 low grade gliomas from Başkent University patients

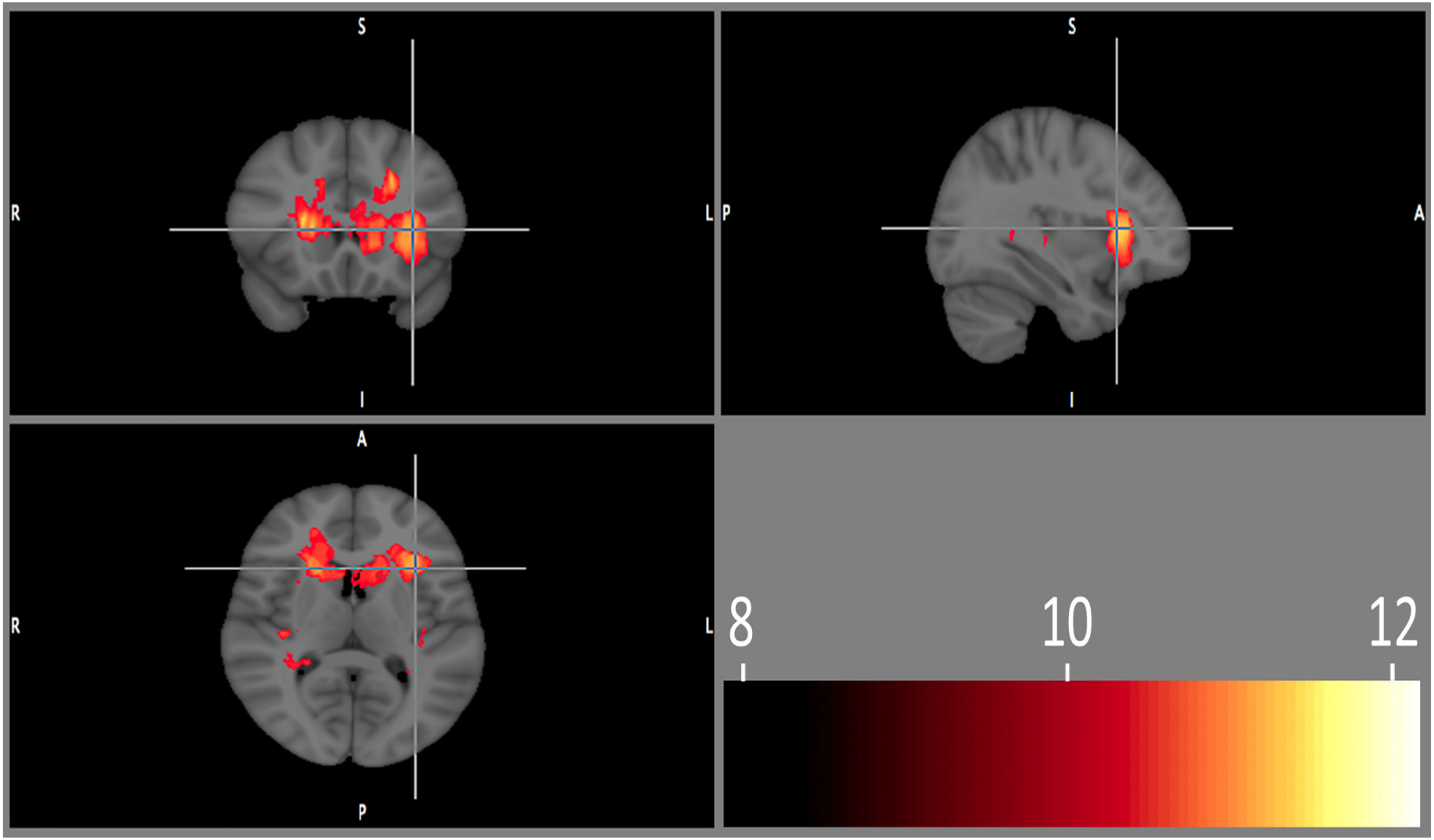

Figure 4.3 Probabilistic brain tumor map of total 132 high and low grade gliomas from Başkent University patients

are mostly located around the occipital horn and nearly left of the ventricular region between 54 low-grade gliomas from Başkent University Hospital as shown in Figure 4.2. Then, the high and low-grade gliomas added together. Since tumor regions are distinct from each other comparing these probabilistic tumor maps, we observed resulting total probabilistic map graph as having very low tumor observing intensities. Nevertheless, it is observed that gliomas are encapsulated around the sub-ventricular zone as in Figure 4.3.

4.2 Probabilistic Brain Tumor Map of REMBRANDT Images

REMBRANDT database provides researchers random brain tumor data in order to investigate in the gliomas deeply. In the thesis, probabilistic brain tumor of REMBRANDT data is generated even though high or low-grade information of gliomas is not maintained. All the same, we observed close relation between resulting probabilistic maps of REMBRANDT gliomas and Başkent University high-grade gliomas. As shown in Figure 4.4, tumors are spread over the right superior part of CSF region.

4.3 Probabilistic Brain Tumor Map of BRATS Images

BRATS images have high glioma observable rates, which is more than 50%. Furthermore, we have just 10 low-grade and 20 high-grade images. These low numbers of images are actually not enough to compose a probabilistic map. Moreover, MICCAI, which is the main resource of data, does not provide the patient reports so that we are unable to reach information about how random the data is. Because the dataset has few patients, when we normalized them with a constant of 0.09 they would have binary intensity thresholds. Hence, it is better to present them without normalization. Even so, we can evaluate the resulting figures and compare them with Başkent data.

In Figure 4.5, we noticed that gliomas are banded together mostly around right

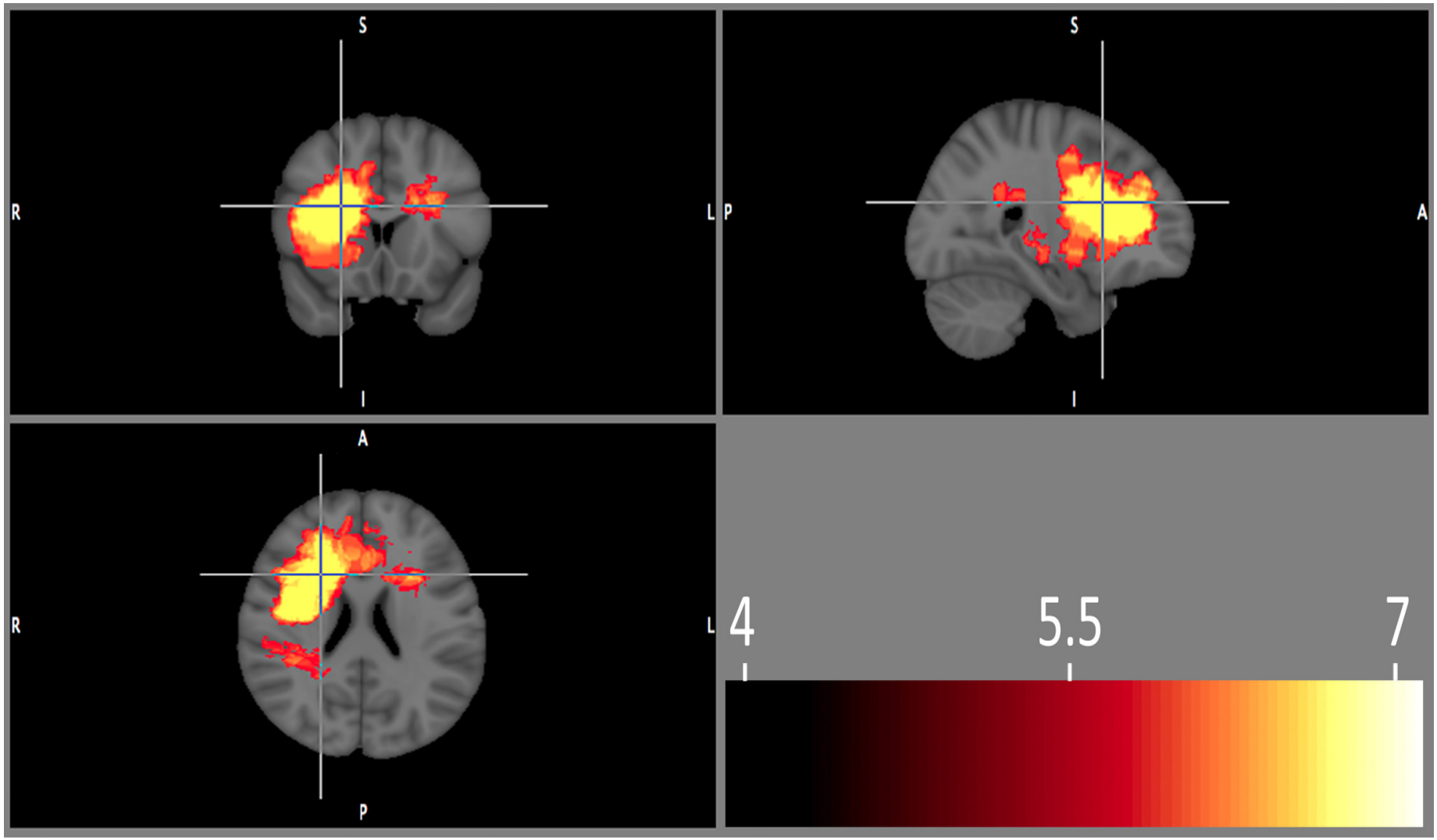

Figure 4.4 Probabilistic brain tumor map of 70 gliomas from REMBRANDT data

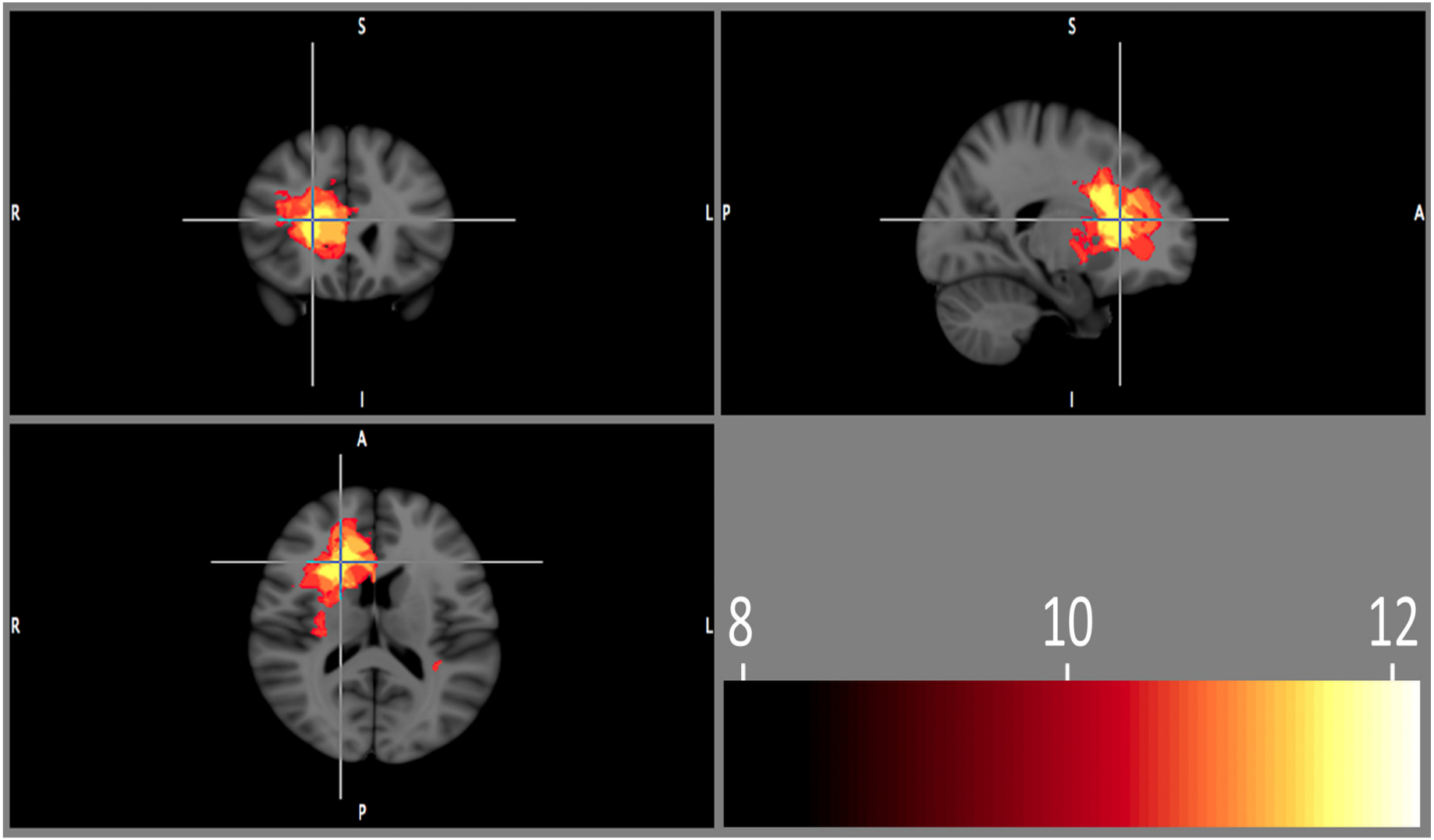

Figure 4.5 Probabilistic brain tumor map of 20 high grade gliomas from BRATS 2012 data

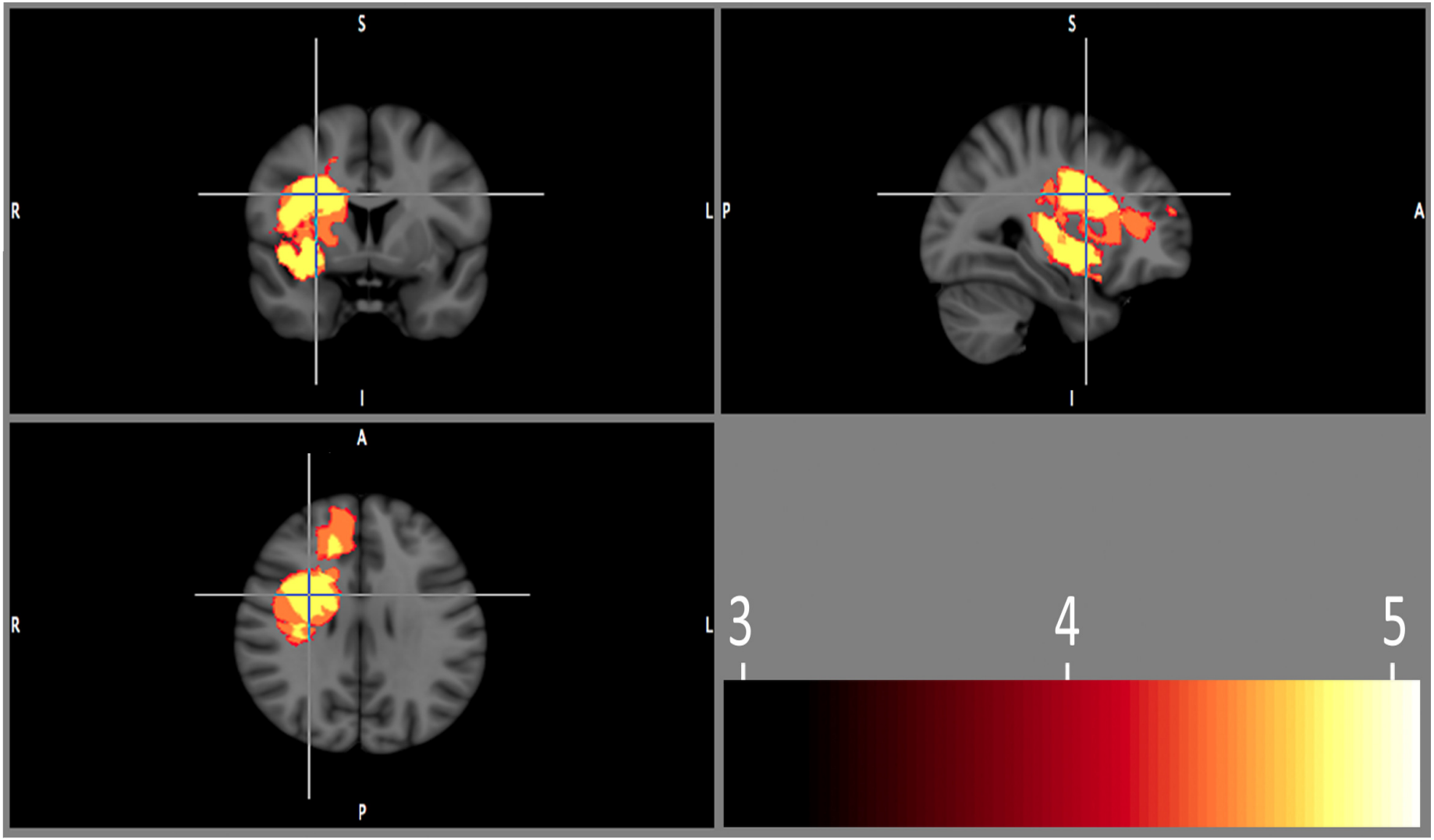

Figure 4.6 Probabilistic brain tumor map of 10 low grade gliomas from BRATS 2012 data

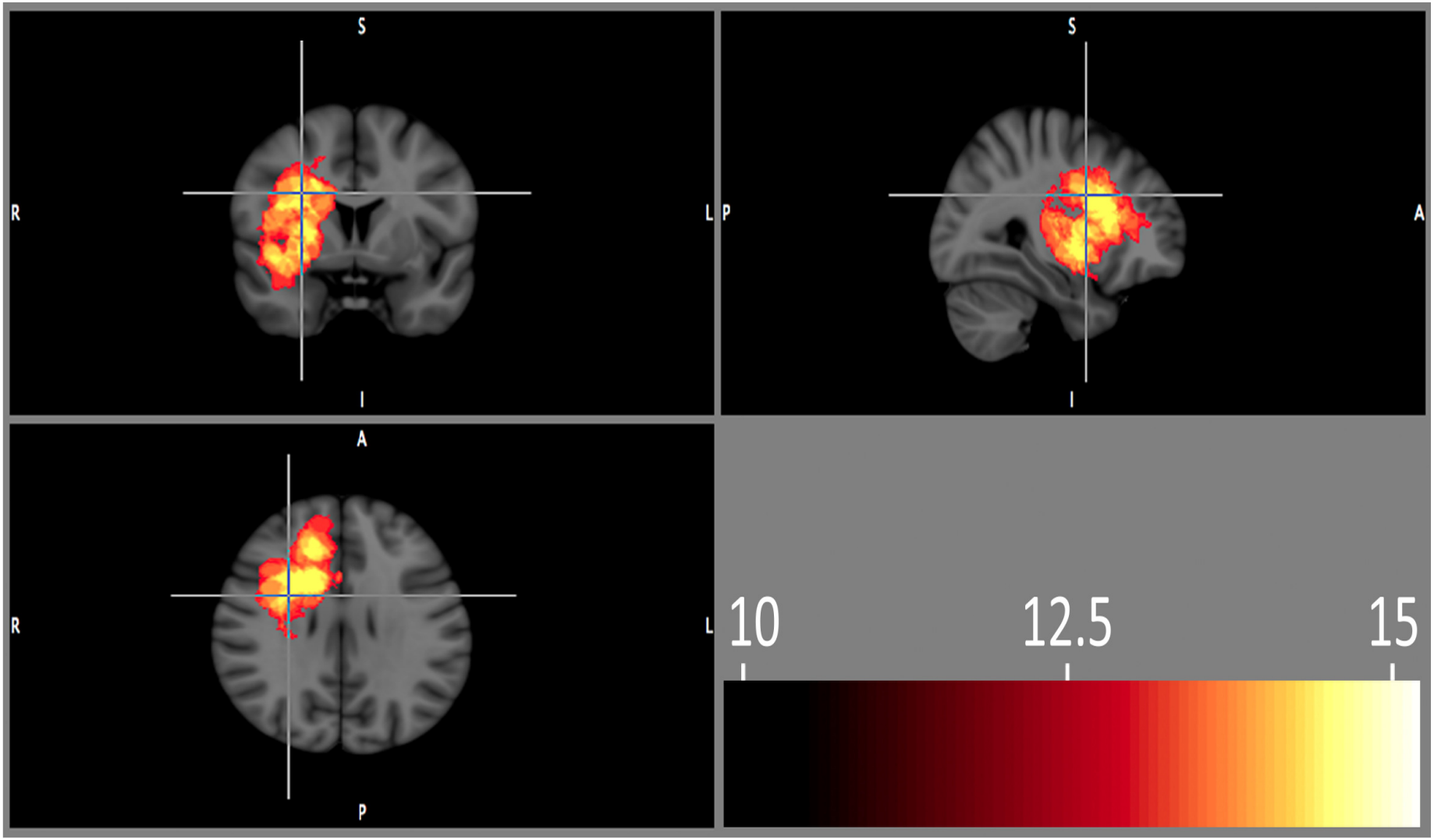

Figure 4.7 Probabilistic brain tumor map of 30 low grade gliomas from BRATS 2012 data

and superior region of the ventricular zone. There are 12 brain tumor patients besides 20 have gliomas in that region of interest. It is very high observing rates as a ratio. Yet it is hopefully observed close circumference area as a high grade glioma map of Başkent dataset.

When the low-grade maps are compared, we come to a different solution from Başkent low-grade images. That's why we have too few data from BRATS 2012, the resulting diagrams differ from each other. Low-grade probabilistic glioma map of BRATS 2012 data, which is shown in Figure 4.2, has tumor regions mostly around the right of the ventricular zone. The total glioma map of 30 patients are presented in Figure 4.3, and the resulting figure is very close to other BRATS 2012 low and high-grade glioma maps. Notice that tumors are again located around the sub-ventricular zone.

4.4 Probabilistic Brain Tumor Map of High & Low Grade Images

High and low-grade maps are generated from the data of Başkent University and Brats separately. We added resulting figures from both data sources together and compared the probabilistic maps of high and low-grade gliomas. For the high-grade map, we gathered totally 98 patients data, which is a sufficient number for a probabilistic map formation.

In Figure 4.8, tumors are encircled around the ventricular region, especially around right and superior part. This result is compatible to above high-grade maps. In addition, the total low-grade probabilistic map also includes tumors mostly around right and upper region of SVZ as in Figure 4.9. Although location of tumors in Başkent University low-grade map was observed on the left side of SVZ comparing sagittal planes, because Brats tumors were highly dense on right and superior region of SVZ, Brats effect on total low-grade map became dominant. To go into detail, Brats low-

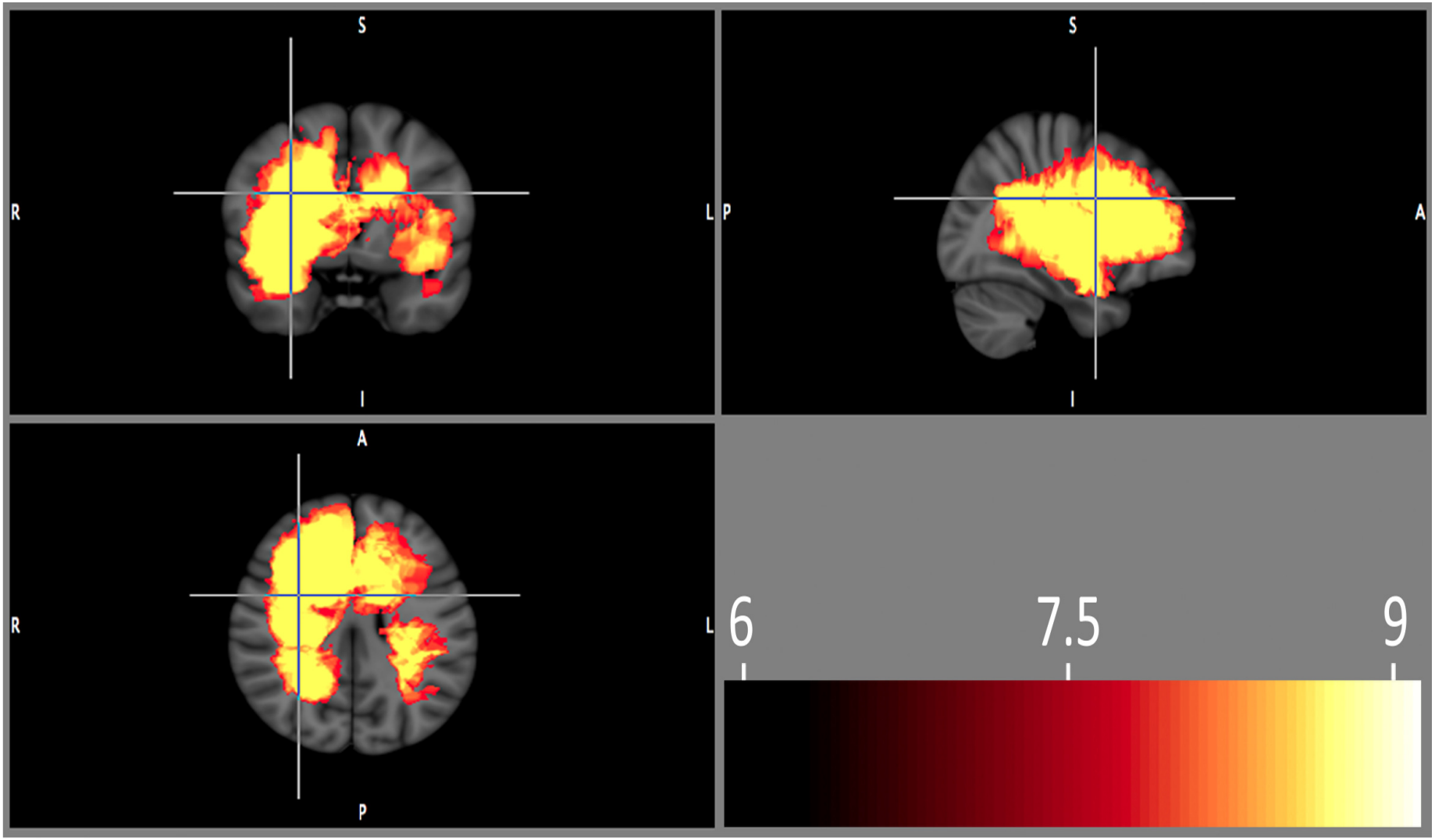

Figure 4.8 Probabilistic brain tumor map of 98 high grade gliomas including Başkent and BRATS 2012 data

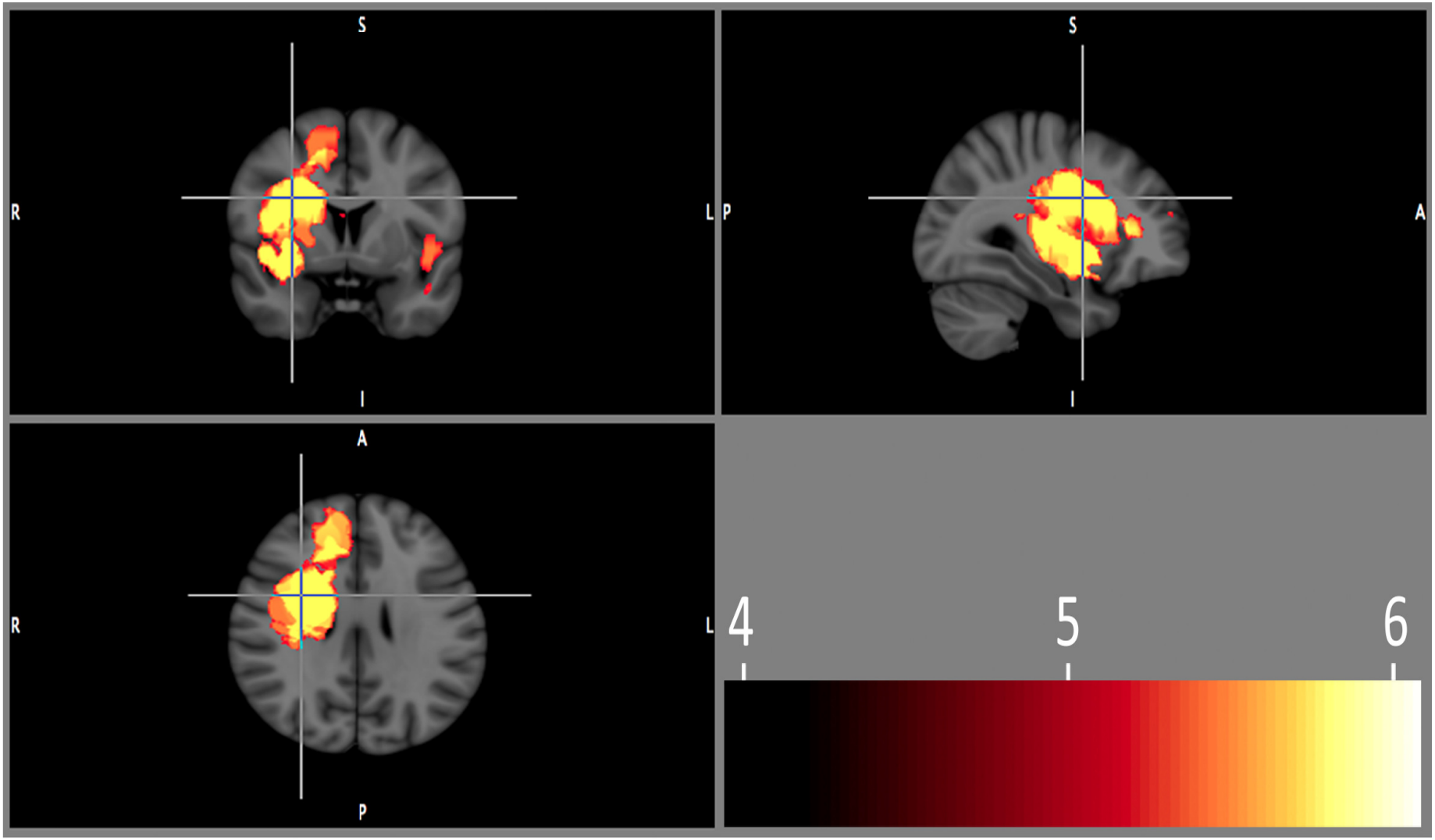

Figure 4.9 Probabilistic brain tumor map of 64 low grade gliomas including Başkent and BRATS 2012 data

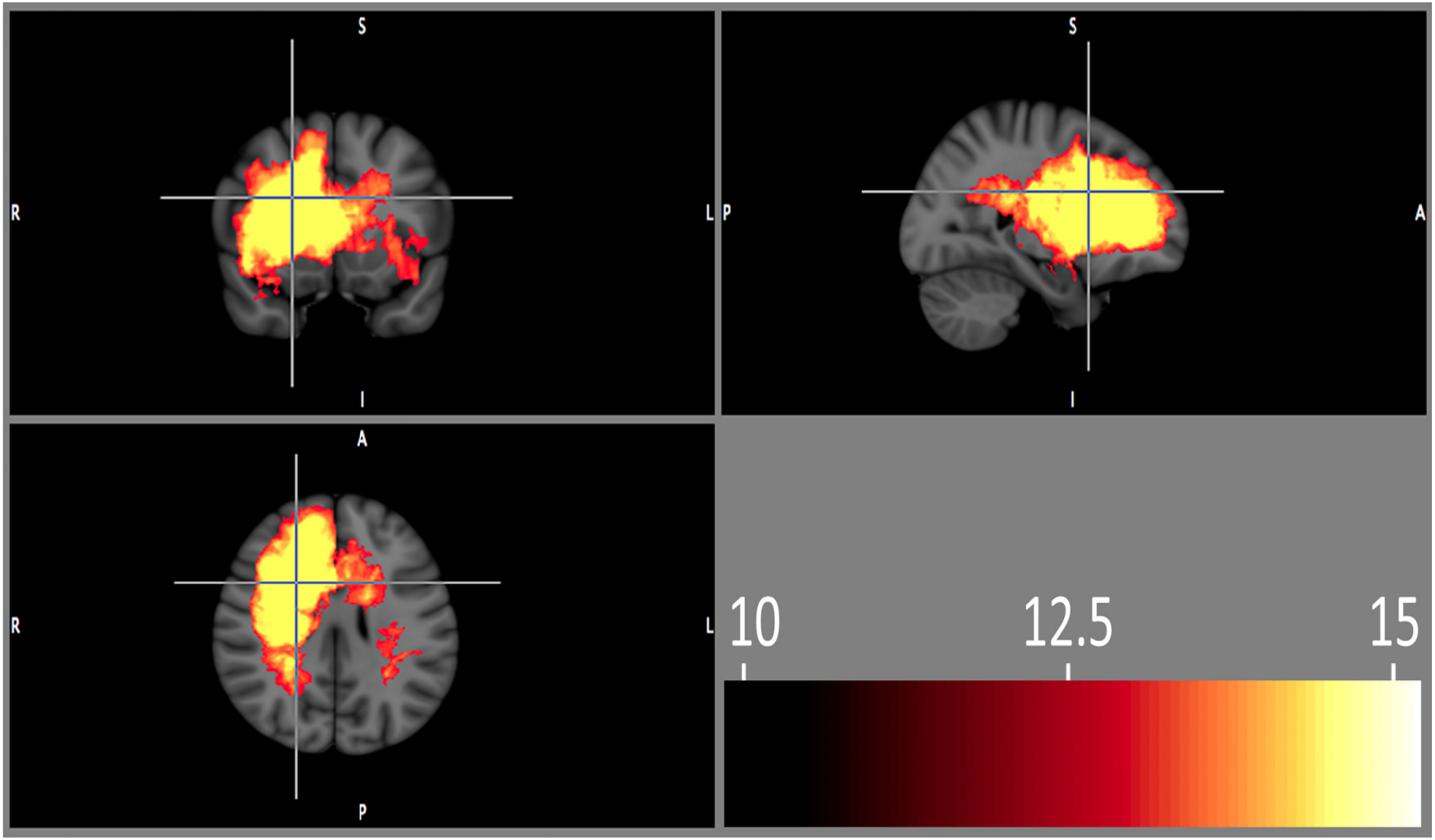

Figure 4.10 Probabilistic brain tumor map of 162 total high and low grade gliomas from total Başkent University and BRATS 2012 data

grade data were composed of 10 images, which is not sufficient number to generate a probabilistic map. Hence it might be better to stick on the result of the low-grade map of Başkent University, which includes more than fifty images. Besides, we combined both low and high-grade maps together, which is indicated in Figure 4.10. The resulting diagram is composed of 162 images, and tumors are predominantly spread over right and superior SVZ.

4.5 Probabilistic Brain Tumor Map of All Images

Finally, we combined all probabilistic maps together, and obtained a brain tumor probabilistic map composing of 232 MRI data through glioma patients. Figure 4.11 indicates tumor-observing regions within the threshold values between 14 and 22. Other brain parts have tumor observing rates less than the threshold value (14); thereby, we may ignore such regions for presenting a probabilistic map generation. Coronal view of this diagram shows that tumors are located on right side while axial view presents that tumors are observed anterior region of the brain essentially. In sagittal view, we observed gliomas commonly around the right and superior field of SVZ.

Başkent University provided us with completely random data. Rembrandt data are also incidentally collected. However, we could not reach information about the randomness of Brats data. It is because tumor observing rates in Brats images are recognized more than 50%, which is extremely higher rate compared to the probabilistic maps from other data resources, we got suspicious about the heterogeneity of glioma regions. Hence, it might be better also to give result of probabilistic map composing of brain tumor patients from Başkent University and Rembrandt that is shown in Figure 4.12. When this figure is compared to the previous one, there is not much difference between graphics in terms of the tumor observing circumferences. But the area of tumors became slimmer. The reason why Brats data is not included in this figure is that the resulting figure is just slightly changed, but hopefully mostly observed tumor regions remained unchanged.

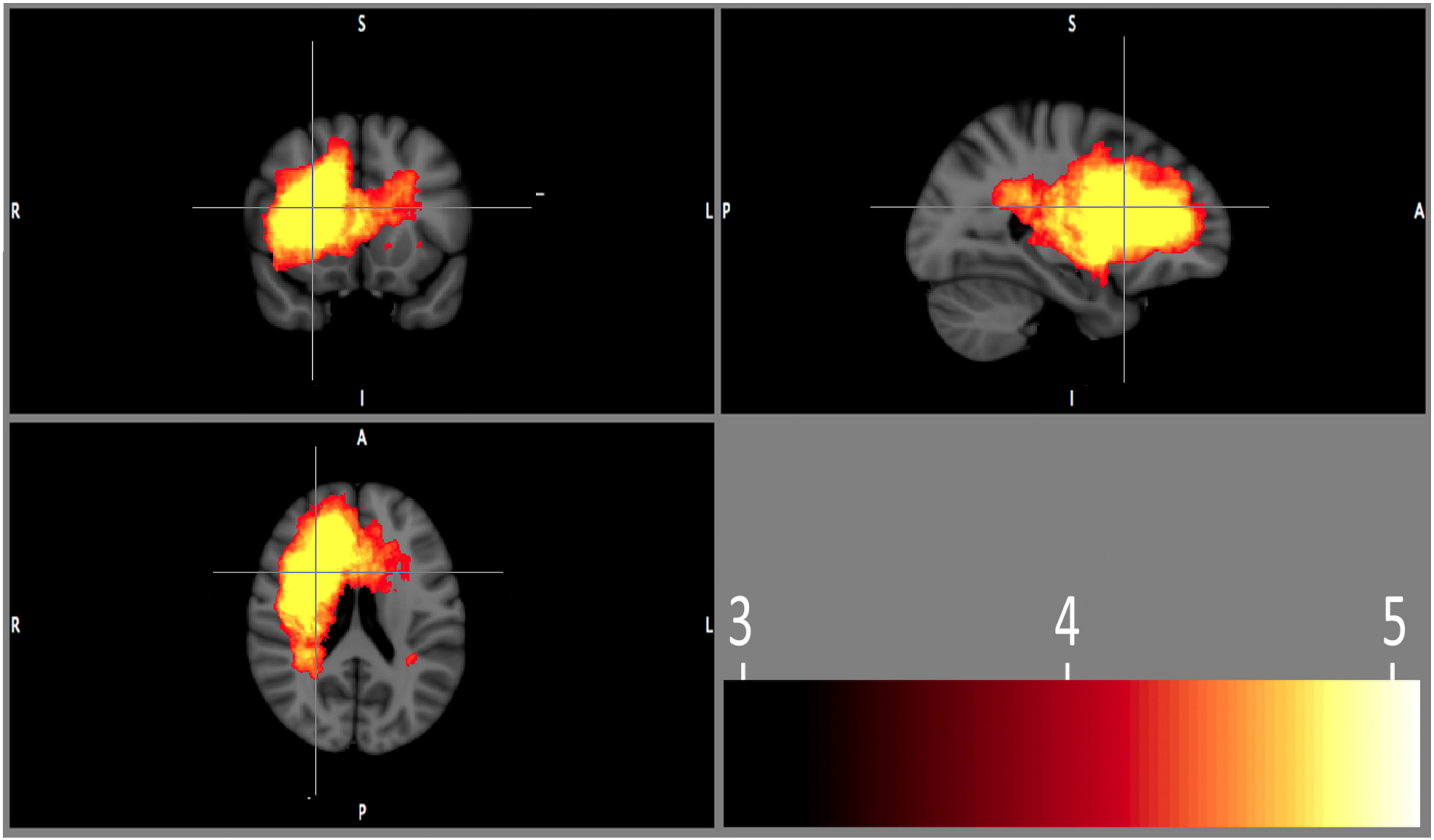

Figure 4.11 Probabilistic brain tumor map of 232 gliomas composing of all data

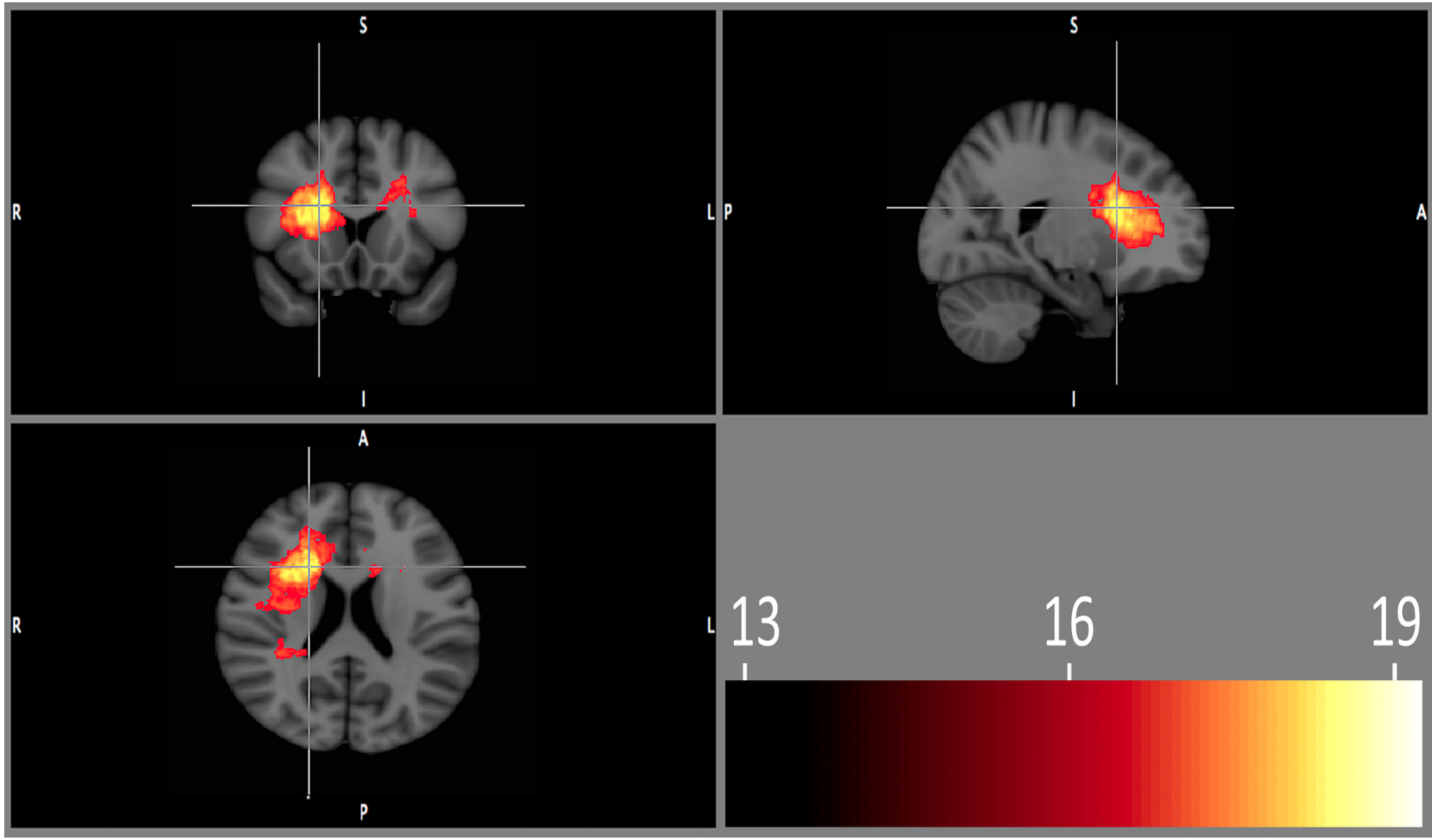

Figure 4.12 Probabilistic brain tumor map of 202 gliomas including data from Başkent University and Rembrandt database

4.6 Overall Evaluation of the Results

For comparison of thesis results from a different angle, we created a table indicating tumor observance frequency comparison in Table 4.2. The table shows the maximum number of the tumors in mostly observed regions for each particular dataset. Moreover, we divided this number to total number of images for each MRI data and obtained the observance rates as percentages. Also note that the probabilistic maps that have tumor-observing rate greater than 9% have more yellow regions than others as it can be examined in above figures.

Table 4.2
Tumor Observance Frequency Comparison.

Data Resource	Data Type	Number of Images	Max # of Observed Tumors	Tumor Observance Rate
Başkent University	HG	78	10	13%
	LG	54	5	9%
	LHG	132	9	7%
BRATS	HG	20	15	75%
	LG	10	5	50%
	LHG	30	12	40%
Başkent University & BRATS	HG	98	25	26%
	LG	64	9	14%
	LHG	162	20	12%
REMBRANDT		70	10	14%
Başkent University & REMBRANDT		202	23	11%
TOTAL		232	30	13%

For Başkent University patients, high grade gliomas are observed with a percentage of 13 whereas low grades are of 9% and their composition map has a percentage of 7. Besides, Rembrandt probabilistic map has also close observing rates with Başkent data, and their combination composing of 202 patients shows that 11% of gliomas are observed around the same region. Likewise the Başkent maps, there is also a slight difference between low and high-grade gliomas such that high-grade glioma observing frequency is higher than the low-grade observing frequency. The same phenomenon is

again observed for the combination of both data resources as 26% for a total high grade map and as 13% for low grade map. When the Figures 4.8 and 4.9 are compared, tumors are observed in different regions, which is right side for high-grade while it stands on left side for low-grade map. Hence, when both maps are added, the combination map must have less tumor observation rates; thereby, the table confirms these figures. Furthermore, tumor observing rates in Brats data are about fifty percentages, which means that one of each two patients have gliomas on the same region. Therefore, it is possible that Brats data are composed of particular types of gliomas.

4.7 The Accuracy Rates of Glioma Type Decision Algorithms

With the use of the probabilistic maps obtained from Başkent University brain tumor patients, we speculated to generate a system which may estimate the brain tumor type. We applied the methods mentioned in Section 3.6.1. We randomly chose 10 high grade gliomas and 10 low-grade gliomas as testing data. The rest of data is put to use for generation of brain tumor maps. We did 32 iterations for the sake of reliability. It means that we picked total 20 random patients and observed the accuracy of the result whether it guessed tumor type right or wrong. We defined an accuracy rate which presents how many patients are estimated truly between 10 high and 10 low-grade brain tumor patients. Then we run the algorithm for another total 20 random patients and saved the result. In this way, we iterated the algorithm 32 times and come up with $32 * 10 = 320$ different accuracy rates for each glioma type. Finally we obtained the mean and standard deviation of these rates.

Normalized dot product comparison algorithm is estimated high grade brain tumors with the success rate of 72% whereas of 53% for low grades. On the other hand, the success rate in center of mass comparison method is only 62% for high grade brain tumor patients and 55% for low-grade brain tumor patients.

Dot product comparison method is succeeding to guess the high-grade gliomas while low grades test data presented very low performance which has fifty-fifty accuracy

rate. The reason behind depressed success rate may be that low-grade gliomas hold contrast agent with a little amount; thereby, they have low intensity values compared to the high-grade gliomas. Since we make dot product of test data with glioma maps and the low-grade tumor region is located narrowly compared to the high-grades as well as the intensity values of low-grades are fewer, the dot product results of low-grade test data are not as high as the dot product results of high-grades. Correspondingly, we obtained low accuracy rates for the estimation of low-grade gliomas.

The method of center-of-mass comparison is misestimated even high-grade gliomas. When the probabilistic high-grade brain tumor map is examined in detail, tumors are gathered in the superior and right lateral region of sub-ventricular zone. When we calculated the center-of-mass of high-grade brain tumors, we hopefully obtain the center inside the SVZ zone, which generally does not include any brain tumors. Because we attained the center-of-mass of brain tumors out of their highly observance regions, the algorithm performs with low quality in the determination of glioma types.

To test the algorithm, we also utilized from k-means clustering method to determine a specific area which separates low-grades from high-grades. We again used total 20 patients as test data, but run the algorithm 2500 times for the sake of reliability. Finally, we obtained 25000 observations from randomly chosen low and high grade test data, and draw the graph as shown in Figure 4.13. K-means algorithm draw a line that separates the observations into two clusters. When we assigned the blue regions as high-grades and red regions as low-grades, the algorithm predicts the glioma type properly with an accuracy rate of 45%, which is a very low estimation rate.

To put all into a nutshell, we have a variety of technical limitations for generation of an estimation algorithm for glioma types. One is that we have just 54 low-grade and 78 high-grade brain tumor patients, which are limited numbers of studies. In addition, the grade 1 gliomas have small dimensions. That's why we are unable to validate the glioma type with high accuracy rates. On the other side, because grade 4 gliomas are large in size, they can be discriminated easily. We need to maintain more data to differentiate grade 2 gliomas from grade 3 gliomas.

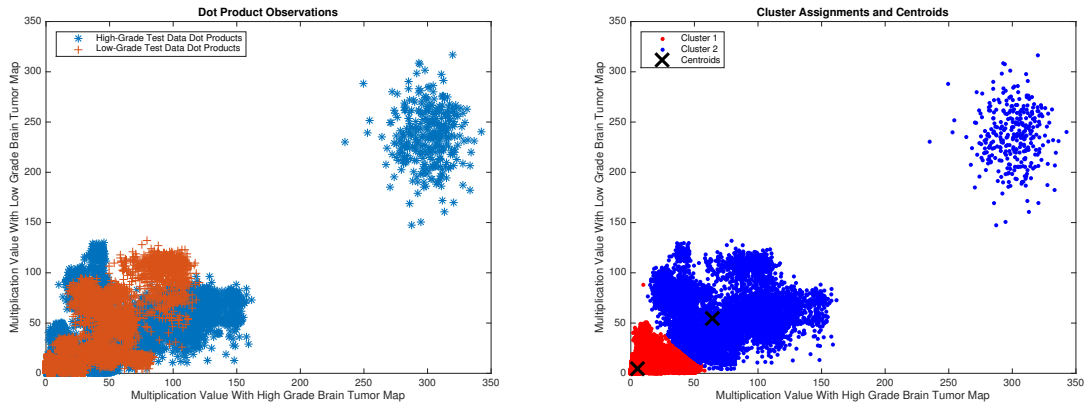

Figure 4.13 Dot product observations (a) and k-means cluster assignments and centroids (b)

As it is mentioned in the introduction part of the results section, all graphics are actually 2D presentation of 3D constructed data. Hence, the reader is unable to see other slices of resulting figures. Moreover, we also underlined that the images are presented in between the intensity threshold levels. That's why we presented the high and low-grade glioma maps from a different perspectives in following images. In Figure 4.14, we did not apply any threshold value to the images.

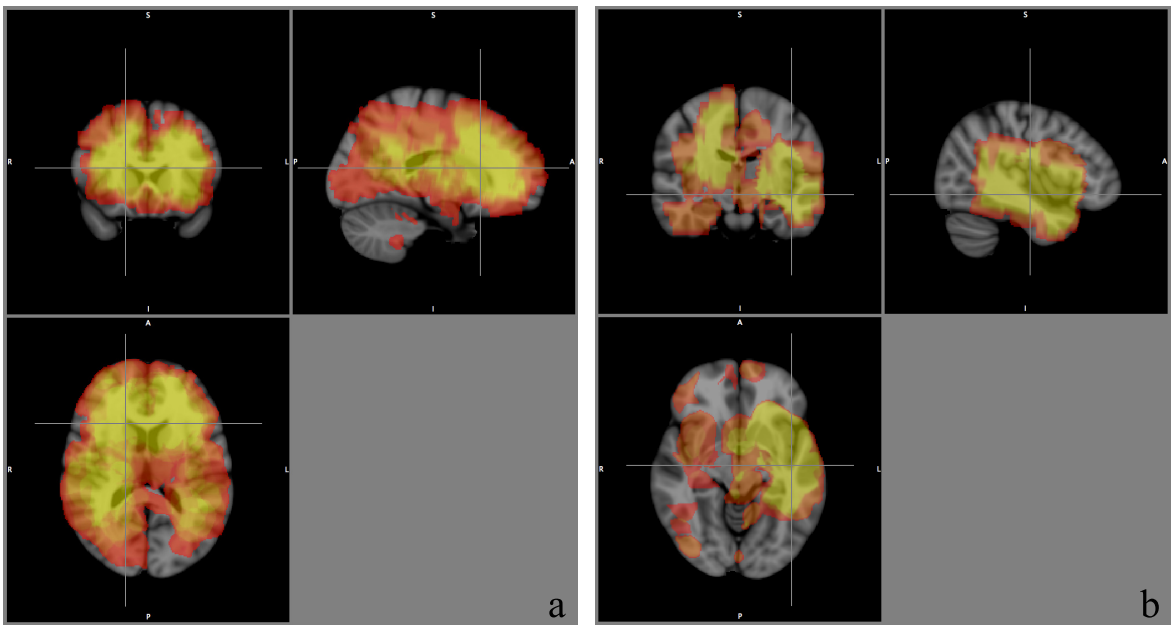

Figure 4.14 High (a) and low (b) grade probabilistic brain tumor maps

In Figure 4.14, high grade tumors are mostly observed around the white mat-

ter tracts as well as sub-ventricular zone. Moreover, low grade tumors are generally gathered around the some of gray matter region. To observe the connection between brain tracts and glioma maps, we registered glioma maps to white and gray matter segmented images of MNI 152 template image.

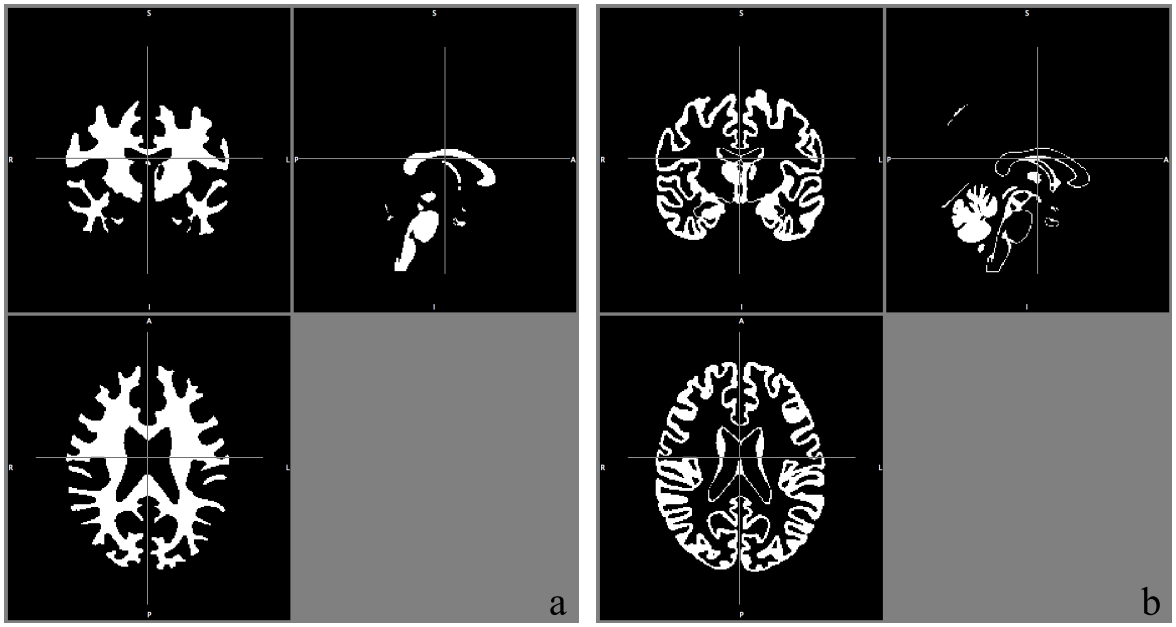

Figure 4.15 White (a) and gray (b) matter segmented images of MNI 152 template image

We registered the resulting high and low-grade glioma maps of Başkent University to the images in Figure 4.15. While there is a slight change after the registration of high grade glioma map to both white and gray matter tracts, low-grade glioma maps are altered dramatically after the registration process. By just looking at the graphics, we may claim that high-grade tumors are mostly located close to the white matter tracts while low-grade tumors do not belong to any of brain tracts.

According to the resulting white and gray matter registered low and high grade maps, we applied dot product comparison method, which is mentioned in Section 3.6.1 in detail. We applied dot product to 78 high grade gliomas with white matter registered high and low grade glioma maps. As a result, we estimated high-grade gliomas properly in 77% of the cases. For 54 low-grade gliomas, we obtained truth rate as just %45. On the other side, we implemented the same method to gray matter segmented glioma

maps. As a consequence, we obtained 69% truth rate for high-grades and 39% for low grades. By looking at the outcomes, we can maintain that the brain tumors are commonly observed closer to the white matter tracts than gray matter tracts.

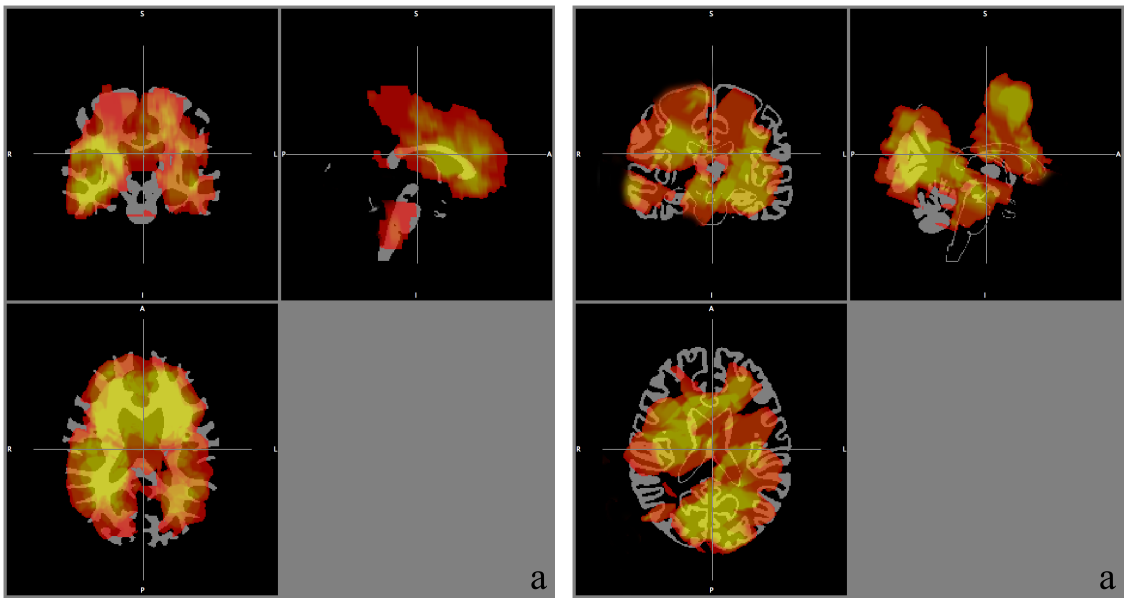

Figure 4.16 White matter registered high (a) and low (b) grade-glioma maps

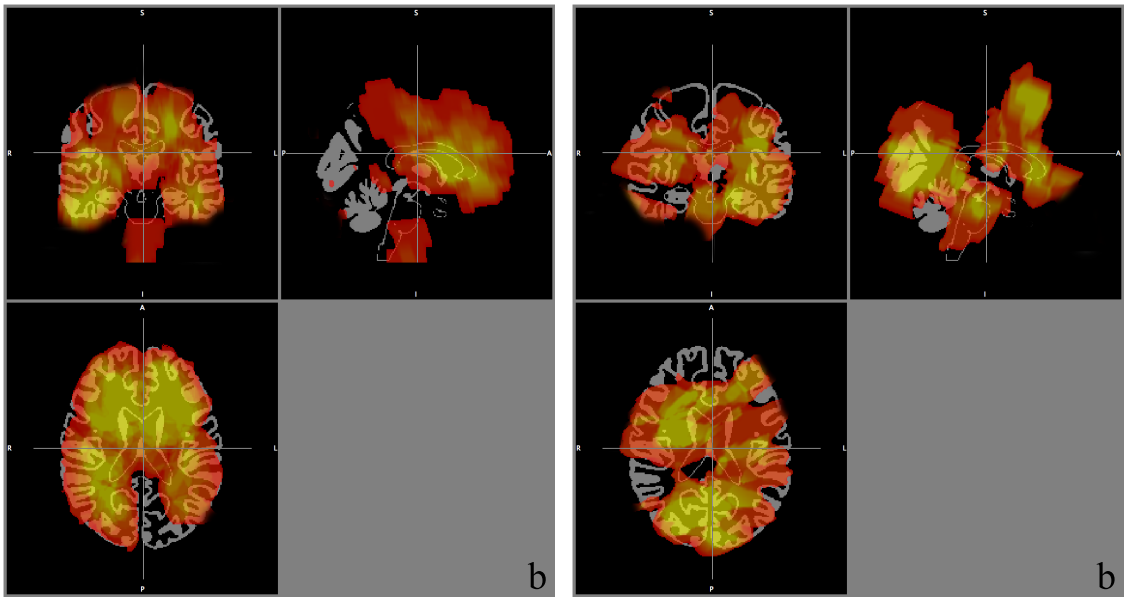

Figure 4.17 Gray matter registered high (a) and low (b) grade-glioma maps

5. CONCLUSIONS AND FUTURE WORK

In this study, all data from different sources are processed to generate the probabilistic glioma maps. We observed a slight difference between resulting probabilistic brain tumor maps of high and low-grade images. Tumors are dispersed all around the right and anterior ventricle zones in low-grades. On the other hand, high-grade tumors have more emerging rates on both sides of ventricle zone, especially in the anterior region.

We attempted to design a system to detect the tumor grade utilizing from the slight difference between resulting low and high grade probabilistic maps. We applied a variety of algorithms including center of mass and k-means clustering algorithm for this purpose. Since we have a limited data for low grade images for the generation of a probabilistic map as well as the sizes and locations of both low and high grade test images are highly complicated, the program resulted in very low accuracy to estimate the tumor grades. Hence, if we could higher number of truth images, the overlap between tumor maps and corresponding test images might increase and this may enable the tumor grade estimation system to work properly.

To put all into a nutshell, all maps indicated that tumors are commonly surrounded over the sub-ventricular region. We also hopefully obtained approximate resulting figures from probabilistic maps composing of low and high-grade gliomas. Figures on results section barely indicate that tumors are observed rarely on cerebellum region of brain while CSF region has generally higher rates of tumor existence suggesting that tumors may arise from stem cells located inside the ventricle. We mentioned about the theory claiming that stem cells are the resource of gliomas in the introduction section. As a result, brain tumor probabilistic maps support this theory.

Physicians implement the radiation therapy treatment around the circumference area after taking out the brain tumor during the operation. We already have an idea

about the spreading region of tumors by virtue of probabilistic glioma maps. As a consequence, in addition to the estimation of originating place of tumors, we may also speculate that physicians should make radiation therapy on the whole tumor and its circumference area so that the tumor may not arise in the same place anymore.

As a future work, the origin of brain tumors can be studied. The group tractography can be generated with the use of fair number of high-resolution diffusion tensor imaging (DTI) dataset. Brain tumor probabilistic maps may be registered to the resulting group tractography. Tumors may use the white matter pathways to spread around the brain tissue. In this way, white matter segmented images that tumors are appearing can be determined. If the gliomas are really originated from the inside of sub-ventricular zone, they are penetrating to the brain in a sort of way. Hence, such a future work may give insight about the determination of both the origin and the pathways of gliomas.

REFERENCES

1. Ostrom, Q. T., H. Gittleman, and et al, "Cbtrus statistical report: Primary brain and central nervous system tumors diagnosed in the united states in 2007 to 2011," *Neuro Oncol*, Vol. 16, 2014.

2. Swanson, K. R., C. Bridge, and et al., "Virtual and real brain tumors: using mathematical modeling to quantify glioma growth and invasion," *J Neurol Sci*, Vol. 216, no. 1, pp. 1–10, 2003.

3. Ellingson, B. M., Lai, and et al., "Probabilistic radiographic atlas of glioblastoma phenotypes," *American Journal of Neuroradiology*, Vol. 34, no. 3, pp. 533–540, 2013.

4. Zlatescu, M. C., A. TehraniYazdi, H. Sasaki, J. F. Megyesi, R. A. Betensky, D. N. Louis, and J. G. Cairncross, "Tumor location and growth pattern correlate with genetic signature in oligodendroglial neoplasms," *Cancer Research*, Vol. 61, no. 18, pp. 6713–6715, 2001.

5. Mandonnet, E., L. Capelle, and H. Duffau, "Extension of paralimbic low grade gliomas: Toward an anatomical classification based on white matter invasion patterns," *Journal of Neuro-Oncology*, Vol. 78, no. 2, pp. 179–185, 2006.

6. Barami, K., A. E. Sloan, A. Rojiani, M. J. Schell, A. Staller, and S. Brem, "Relationship of gliomas to the ventricular walls," *Journal of Clinical Neuroscience*, Vol. 16, no. 2, pp. 195–201, 2009.

7. Sanai, N., A. Alvarez-Buylla, and M. S. Berger, "Neural stem cells and the origin of gliomas.," *The New England journal of medicine*, Vol. 353, no. 8, pp. 811–822, 2005.

8. Alvarez-Buylla, A., and J. M. García-Verdugo, "Neurogenesis in adult subventricular zone," *The Journal of neuroscience*, Vol. 22, no. 3, pp. 629–634, 2002.

9. Galli, R., E. Binda, and et al., "Isolation and characterization of tumorigenic, stem-like neural precursors from human glioblastoma," *Cancer Research*, Vol. 64, no. 19, pp. 7011–7021, 2004.

10. Cap, M., E. Gescheidtova, P. Marcon, and K. Bartusek, "Automatic Detection and Segmentation of the Tumor Tissue," in *Progress In Electromagnetics Research Symposium Proceedings*, pp. 53–56, 2013.

11. Hamamci, A., N. Kucuk, K. Karaman, K. Engin, and G. Unal, "Tumor-cut: Segmentation of brain tumors on contrast enhanced mr images for radiosurgery applications," *IEEE Transactions on Medical Imaging*, Vol. 31, no. 3, pp. 790–804, 2012.

12. Porz, N., S. Bauer, A. Pica, and et al., "Multi-modal glioblastoma segmentation: Man versus machine," *PLoS ONE*, Vol. 9, no. 5, 2014.

13. Boxerman, J. L., K. M. Schmainda, and R. M. Weisskoff, "Relative cerebral blood volume maps corrected for contrast agent extravasation significantly correlate with glioma tumor grade, whereas uncorrected maps do not," *American Journal of Neuroradiology*, Vol. 27, no. 4, pp. 859–867, 2006.

14. Sumanaweera, T. S., Adler, and et al., "Characterization of spatial distortion in magnetic resonance imaging and its implications for stereotactic surgery," *Neurosurgery*, Vol. 35, no. 4, pp. 696–704, 1994.

15. Myers, W. R., M. Möß le, and J. Clarke, "Correction of concomitant gradient artifacts in experimental microtesla MRI," *Journal of Magnetic Resonance*, Vol. 177, no. 2, pp. 274–284, 2005.

16. Wang, J., W. Mao, and et al., "Factors influencing flip angle mapping in MRI: RF pulse shape, slice-select gradients, off-resonance excitation, and B0 inhomogeneities," *Magnetic Resonance in Medicine*, Vol. 56, no. 2, pp. 463–468, 2006.

17. Hattingen, E., and U. Pilatus, *Brain Tumor Imaging*, Springer-Verlag Berlin Heidelberg, 2015.

18. Hornak, J. P., *The Basics of MRI*, 2014.

19. Jenkinson, M., C. F. Beckmann, T. E. Behrens, M. W. Woolrich, and S. M. Smith, "FSL," *Neuroimage*, Vol. 62, pp. 782–790, 2012.

20. Woolrich, M. W., S. Jbabdi, B. Patenaude, M. Chappell, S. Makni, T. Behrens, C. Beckmann, M. Jenkinson, and S. M. Smith, "Bayesian analysis of neuroimaging data in FSL.," *NeuroImage*, Vol. 45, no. 1 Suppl, 2009.

21. Smith, S. M., S. M. Smith, Jenkinson, and et al., "Advances in functional and structural MR image analysis and implementation as FSL.," *NeuroImage*, Vol. 23 Suppl 1, pp. S208–19, 2004.

22. Friston, K. J., J. T. Ashburner, S. J. Kiebel, T. E. Nichols, and W. D. Penny, *Statistical Parametric Mapping: The Analysis of Functional Brain Images*, Vol. 8, 2007.

23. Yushkevich, P. A., J. Piven, H. C. Hazlett, R. G. Smith, S. Ho, J. C. Gee, and G. Gerig, "User-guided 3D active contour segmentation of anatomical structures: Significantly improved efficiency and reliability," *NeuroImage*, Vol. 31, no. 3, pp. 1116–1128, 2006.

24. Smith, S. M., "Fast robust automated brain extraction," *Human Brain Mapping*, Vol. 17, no. 3, pp. 143–155, 2002.

25. Davatzikos, C., J. L. Prince, and R. Nick Bryan, "Image registration based on boundary mapping," *IEEE Transactions on Medical Imaging*, Vol. 15, no. 1, pp. 112–115, 1996.

26. Demir, A., "Anatomical landmark based registration of contrast enhanced-t1 weighted magnetic resonance images," Master's thesis, Sabanci University, Istanbul, Turkey, 2010.

27. Jenkinson, M., and S. Smith, "A global optimisation method for robust affine registration of brain images," *Medical Image Analysis*, Vol. 5, no. 2, pp. 143–156, 2001.

28. Jenkinson, M., P. Bannister, M. Brady, and S. Smith, "Improved optimization for the robust and accurate linear registration and motion correction of brain images," *NeuroImage*, Vol. 17, no. 2, pp. 825–841, 2002.

29. Menze, B. H., A. Jakab, and et al., "The Multimodal Brain Tumor Image Segmentation Benchmark (BRATS)," *IEEE TMI*, pp. 1–32, 2014.

30. Collins, D., C. Holmes, T. Peters, and A. Evans, "Automatic 3-D model-based neuroanatomical segmentation," *Human Brain Mapping*, Vol. 208, no. 1995, pp. 190–208, 1995.

31. Mazziotta, J., A. Toga, and et al., "A probabilistic atlas and reference system for the human brain: International Consortium for Brain Mapping (ICBM).," *Philos Trans R Soc Lond B Biol Sci*, Vol. 356, no. 1412, pp. 1293–1322, 2001.